JGR Oceans

RESEARCH ARTICLE
10.1029/2019JC015333

Key Points:
- The relationship between oceanic eddies and SLPVW volume in winter is influenced by the eddy vorticity strength
- The subduction rate varies greatly from year to year, suggesting the role of the interannual variation of eddies
- In summer, water converges in the composite cyclone, which is beneficial to the retention of the SLPVW

Supporting Information:
- Supporting Information S1

Correspondence to:
H.-B. Hu,
huhaibo@nju.edu.cn

Citation:
Wen, Z., Hu, H., Song, Z., Bai, H., & Wang, Z. (2020). Different influences of mesoscale oceanic eddies on the North Pacific subsurface low potential vorticity water mass between winter and summer. *Journal of Geophysical Research: Oceans*, *125*, e2019JC015333. https://doi.org/10.1029/2019JC015333

Received 29 MAY 2019
Accepted 6 DEC 2019
Accepted article online 20 DEC 2019

Different Influences of Mesoscale Oceanic Eddies on the North Pacific Subsurface Low Potential Vorticity Water Mass Between Winter and Summer

Zhibin Wen[1,2], Haibo Hu[1,3], Zhenya Song[2], Haokun Bai[1], and Ziyi Wang[1]

[1]CMA-NJU Joint Laboratory for Climate Prediction Studies, Instituted for Climate and Global Change Research, School of Atmospheric Science, Nanjing University, Nanjing, China, [2]First Institute of Oceanography, Ministry of Natural Resources, Qingdao, China, [3]KLME and CIC-FEMD, Nanjing University of Information Science and Technology, Nanjing, China

Abstract The generation and dissipation of North Pacific subsurface low potential vorticity water mass (SLPVW) affect various ocean-atmosphere dynamic and thermodynamic processes on a wide range of time scales. Mesoscale oceanic eddies are believed to play an important role in the variation of SLPVW. National Centers for Environmental Prediction (NCEP)/NCEP-Climate Forecast System Reanalysis coupled data set during 1979–2010 has been analyzed to investigate the different influences of mesoscale oceanic eddies on the SLPVW between winter and summer. It is found that the correlation between the sea surface height and SLPVW volume in winter is positive on the north of 30°N but negative on the south of 30°N, which is mainly caused by the eddy vorticity strength. The negative correlation value region has more strong anticyclones than the positive correlation value region, so the mixed layer depth in the negative (positive) correlation value region tends to be deeper (shallower) caused by stronger (weaker) anticyclones, which leads to the decreasing (increasing) of the low PV water mass under mixed layer depth (namely, SLPVW). Eddies also have obvious impacts on the subduction rate. The climatological eddy subduction rate can reach to 1.88 Sv in the NCEP-Climate Forecast System Reanalysis, which accounts for 36.4% of the total subduction rate. In summer, the correlation between the sea surface height and SLPVW volume is remarkably negative. It is found that water diverges (converges) in the composite anticyclone (cyclone), which leads to the increasing (decreasing) of PV value in the composite anticyclone (cyclone), finally accelerates (hinders) the dissipation of SLPVW.

Plain Language Summary The study researched different influences of mesoscale oceanic eddies on the North Pacific subsurface low potential vorticity water mass (SLPVW) between winter and summer. The results revealed that eddies influence the formation of low potential vorticity water by changing turbulent heat flux in winter. Moreover, it is found that the relationship between oceanic eddies and SLPVW volume is influenced by the eddy vorticity strength. The mixed layer depth in the stronger (weaker) anticyclones tends to be deeper (shallower), which leads to the increasing (decreasing) of the low PV water mass but decreasing (increasing) of the low PV water mass under mixed layer depth (namely, SLPVW). The subduction rate varies greatly from year to year, suggesting the role of the interannual variation of eddies. In summer, the rotation of the eddies leads to the convergence and divergence, thus changing the stratification of the ocean and ultimately affecting the dissipation of SLPVW. The results might give the new insight to studies the role of mesoscale eddies on SLPVW, which have important implications for North Pacific climate scientists and predictions.

1. Introduction

Subsurface low potential vorticity water (SLPVW), which is characterized by nearly vertically homogeneous temperature and salinity distributions, is formed in late winter deep mixed layer (ML). Subtropical mode water (STMW) is one of the widely studied SLPVW. In winter subtropical ocean basin, there is a large oceanic heat loss due to the atmospheric cooling over the warm sea surface, especially over the warm side of the Kuroshio or Gulf Stream fronts (Chen et al., 2019; Bai et al., 2019). The deep convective mixing which is relevant to the wind stress and oceanic heat loss, makes the mixed layer depth (MLD) reaching the maximum in late winter. At this time, the low potential vorticity (PV) water masses are formed in deep ML on the warm side of a strong current or front (Qiu, Hacker et al., 2006; Oka & Qiu, 2012). Subsequently, as the MLD

rapidly becomes shallow, the lower part of the deep ML is separated from the upper by the seasonal thermocline, which is rapidly formed in the early spring. The effects of the atmosphere on the water masses have been isolated and preserved. Some of the low PV water masses eventually enter and remain in the permanent thermocline, which are called mode water (Stommel, 1979), and this process is called subduction (Stommel, 1979; Marshall et al., 1993). There are three main types of mode waters formed in the subtropical North Pacific: the western STMW (Masuzawa, 1969), the eastern (STMW) (Hautala & Roemmich, 1998), and the central mode water (Nakamura, 1996; Suga et al., 1997). The STMW proposed by Masuzawa (1969) is usually used to refer to the Western Subtropical Mode Water. It is a distinct water mass between the seasonal thermocline and the permanent thermocline, with relatively weak stratification. The northern boundary of STMW is near 34.5°N, the southern boundary is 30°N or farther, the eastern boundary is at 151.5°E, and the western boundary up to 140°E or farther.

After subduction, mode water moves along the isopycnal and diffuses to other areas and affects the dynamic and thermal processes. STMW is found to be advected southwestward, carrying its temperature and salinity anomalies to the western boundary. Then, it may turn back the formation area by Kuroshio Stream. Moreover, STMW obducts into ML and affects the sea surface temperature (SST) of the formation area. This process has been proved to be a possible negative feedback mechanism responsible for the Pacific Decadal Oscillation (Qiu & Huang, 1995; Qiu, 2002; Endoh et al., 2006; Liu & Hu, 2007). Chang and Zhang (2010) proposed that the summer mode water anomalies can impose an effect on the autumn-winter air temperature over China by the anomalous patterns of the Asian-Pacific atmospheric circulation and the SST anomalies over the Kuroshio area. Recent enhanced observations and model simulations have revealed the importance of mode water in the formation and variability of North Pacific subtropical countercurrent (Xie et al., 2011; Xu et al., 2012; Kobashi & Kubokawa, 2012). Moreover, mode water are believed to play an important role in biogeochemical processes such as the oceanic uptake of atmospheric CO_2 (Bates et al., 2003) and the nutrient cycling in the oligotrophic subtropical gyres (Kremeur et al., 2009; Sukigara et al., 2011).

Changes in the mixing process of upper oceans lead to a significant seasonal variation in STMW. The effective time of the low PV water masses entering the permanent pycnocline through the ML (namely, subduction) is very short. It generally only occurs in the late winter and early spring (Marshall et al., 1993). After the subduction, the thickness of STMW reaches the maximum in March or April. With the emergence of seasonal thermocline, no new STMW generates, and the thickness of the already generated STMW is gradually reduced until another winter. This is called the annual cycle of STMW changes (Song et al., 2009).

The subtropical northwestern Pacific with the Kuroshio Extension (KE), which is the largest heat loss area, is an important thermocline ventilated region. It also has frequent eddy activity, high eddy kinetic energy (EKE), and the most active ocean-atmosphere interaction in the subtropical ocean (Qiu, 2002). In recent years, based on Argo buoy data and long-term satellite observation data, there are much clearer understandings of the generation, transport, and dissipation of STMW. The change of STMW is closely related to the oceanic currents, fronts and mesoscale eddies. The process of formation and migration of STMW is inevitable affected by the oceanic eddies.

It is found that the generation and subduction of STMW are modulated by mesoscale oceanic eddies: Since anticyclones (cyclones) are usually accompanied by deeper (shallow) permanent pycnocline and weaker (stronger) background stratifications, more STMW tends to generate in anticyclones (cyclones) (Uehara et al., 2003; Pan & Liu, 2005; Rainville et al., 2007; Nishikawa et al., 2010; Kouketsu et al., 2011). However, the most previous conclusions are based on analysis of the Argo buoy case, which may be biased by preference for strong eddies. Pan and Liu (2005) analyzed the effects of mesoscale oceanic eddies in the STMW formation region on the winter ML, based on the Argo buoy data from the Kuroshio recirculation region in February and March 2001. It is found that existence of the eddy greatly changes the local heat loss of the sea surface. Anticyclones cause a large amount of local heat loss, which can enhance the vertical mixing process, forming deeper ML and thermocline, which contributes to the generation of STMW, while cyclones have the opposite effect. Qiu, Chen et al. (2006) proposed that the interannual variation of STMW is related to the occurrence of Kuroshio Large Meander. When Kuroshio Large Meander occurred, unusually strong cyclones brought the high PV water of the KE into the ML, consequently the stratification of the upper ocean is strengthened, and the formation of deep ML and the generation of STMW are

suppressed or the high PV water mass is directly injected into the low PV water mass, resulting in small STMW volume. Eddy advection significantly affects the subduction of STMW (Xu et al., 2014; Xu et al., 2016). Since anticyclones cause the low PV water masses to migrate southward and cross the winter mixed layer front, finally subduct into permanent pycnocline. The contribution by mesoscale oceanic eddies accounts for about 50% of the total subduction rate (Nishikawa et al., 2010).

Mesoscale oceanic eddies not only affect the STMW in the generation season (late winter and early spring) but also affect STMW distribution in the non-generation season. STMW is thicker in the anticyclone and thinner in the cyclone (Rainville et al., 2007; Nishikawa et al., 2010; Oka et al., 2011). Those eddies with a strongly nonlinear nature can trap a substantial amount of mode water within them during their southwestern movement (Flierl, 1981; Uehara et al., 2003; Xu et al., 2017). Rainville et al. (2007) found that the mesoscale oceanic eddy dominates the transport of STMW to the south of 26°N, which is about 2.56 Sv, while contribution of the mean flow is only 0.4 Sv. Nishikawa et al. (2010) found that the anticyclone carries STMW to the south at the southern boundary of the STMW source that direction is perpendicular to the mean flow. Two possible local processes are suggested. One is the eddy mixing of PV by eddy flow in the presence of a large PV gradient, which leads to the southward transport of low PV mass. The other is the southward translation of the anticyclone itself, which accompanies large volume of low PV water. Shi et al. (2018) compared the differences between different mesoscale oceanic eddies based on the shape of their isopycnals in transporting the STMW. Liu and Peiliang (2013) found that in the nongeneration months (from May to Dec), the "trapped depth" of the anticyclone is deeper than that of the cyclone, namely, the anticyclone can trap thicker STMW to its center and then transports it southward.

In the previous studies, the time span of nongeneration months was too long (including late spring, summer, autumn, and early winter), and the effects of upper oceans on SLPVW could not be completely isolated in late spring and early winter. The time-averaged MLD in summer is only 18.3 m, while the SLPVW mainly exists in the depth range of 100–250 m. At this time, the dissipation and transportation of the SLPVW are hardly affected by the upper ocean but significantly affected by the mesoscale oceanic eddies. How does the summer mesoscale oceanic eddies affect the SLPVW? Is there a corresponding relationship between the distribution of summer SLPVW and mesoscale oceanic eddies in the statistics? What kind of mechanism maintain this correspondence? What is the difference between the summer and winter mesoscale oceanic eddies affecting SLPVW?

In order to solve this series of questions, this paper will use the National Centers for Environmental Prediction Climate Forecast System Reanalysis (NCEP-CFSR) 6-hourly data to study the long-term winter and summer SLPVW and mesoscale oceanic eddies in subtropical North Pacific. The rest of this paper is organized as follows: Section 2 briefly describes the data and calculation methods used in this paper, especially the definition of SLPVW and different subduction rates; section 3 analyzes the correlation between SLPVW and subtropical North Pacific mesoscale oceanic eddies in winter and summer, respectively; section 4 composites eddies and describes the mechanism that eddies impact on SLPVW in winter; section 5 composites eddies and describes the mechanism that eddies impact on SLPVW in summer; and section 6 offers summary and discussion.

2. Data and Method

The climatological eddy diameter is about 200 km in the eddy-rich low and middle latitude regions (Chelton et al., 2007); therefore, the NCEP-CFSR 6-hourly earth-system data with the 0.5° × 0.5° spatial resolution should be enough to detect eddies. The NCEP-CFSR Selected Hourly Time-Series Products (ds093.0) last 32 years from 1979 to 2010, the time resolution is 6 hr, and the spatial horizontal resolution is 0.5° × 0.5°. The NCEP-CFSR oceanic data used in this study has 40 levels from 5 to 4,478 m. The NCEP-CFSR atmospheric data has multiple vertical coordinates, 2-m temperature, 10-m winds, and sea surface heat flux are used in our study. NCEP-CFSR was designed and executed as a global, high-resolution coupled atmosphere–ocean–land surface–sea ice system to provide the best estimate of the state of these coupled domains over this period (Saha et al., 2010). The NCEP-CFSR data is characterized by global coverage, high spatial and temporal resolution, and abundant oceanic data sources. It can be used for the study of mesoscale oceanic ocean phenomena, and it is conducive to improving the accuracy of SLPVW research. In order to overcome the shortcomings of the NCEP-CFSR data in spatial resolution, the data is bilinearly

interpolated, the spatial horizontal resolution after interpolation is 0.25° × 0.25°. All the correlation analysis and eddy composition analysis use daily mean data. And similar results are calculated from year 2001 to 2010 or during years 1979–2010 using NCEP-CFSR data.

NCEP-CFSR is an ideal data product with its spatial and temporal continuous distribution and provides the data of flux field which can reflect the relationship between turbulent heat flux and SLPVW. However, the horizontal resolution of NCEP-CFSR data may be questioned whether it is enough to catch the detail structures of each eddy. To make the results more convincing, we add analyses of a higher resolution global assimilation data (Global HYbrid Coordinate Ocean Model and the Navy Coupled Ocean Reanalysis Data-GLBv0.08/expt_53.X) to confirm the results shown in the present study. The time resolution of HYCOM/NCODA Global Reanalysis Data is 3 hr. The spatial resolution is 0.08° resolution between 40°S and 40°N but 0.04° poleward of these latitudes in horizontal, which has 40 levels in vertical from 0 to 5,000 m. For comparison, the data is bilinearly interpolated to 1/6° × 1/6°, and all the analysis in the discussion use daily mean data from 2001 to 2010. It should also be mentioned that although the spatial resolution of the HYCOM/NCODA data is higher, it is only the product of the global ocean circulation model driven by sea surface forcing.

In this study, MLD is defined as the depth corresponding to the potential density higher than the sea surface of 0.125 σ_θ.

PV value is regarded as a good index for studying the generation and migration of SLPVW. In this study, PV is calculated by its definition as follows:

$$q = \frac{f}{\rho}\frac{\Delta\sigma_\theta}{\Delta z} \tag{1}$$

where f is the Coriolis parameter, ρ is density, $\frac{\Delta\sigma_\theta}{\Delta z}$ is the vertical gradient of potential density, and Δz is 10 m in this study. We define SLPVW as water that with PV less than or equal to 2×10^{-10} m^{-1} s^{-1} and lying below the ML. The SLPVW volume is defined as the number of grids in the vertical direction (5- to 395-m interval of 10 m), which meet the above conditions.

The local instantaneous subduction rate s is given by

$$s = -w - u\cdot\nabla h_b \tag{2}$$

where $\bigtriangledown h_b$ is the horizontal gradient of maximum MLD and u and w are the horizontal and vertical velocity at the base of the annual maximum MLD. The annual subduction rate of a density range ($\sigma_a < \sigma < \sigma_b$) is calculated by regionally and temporally integrating s:

$$S(\sigma_a<\sigma<\sigma_b) = \frac{1}{T}\int_0^T \sum_{i,j} s_{i,j}(t)\Big|_{\sigma_a<\sigma<\sigma_b} \Delta A_{i,j}\,dt \tag{3}$$

Here (i, j) is the horizontal grid index, ΔA is the area of a grid, t is time, and T is the averaging period, which is February and March per year. The integration region is depicted in Figure 2, and the potential density of mode water ranges from 24.8σ_θ to 25.3σ_θ. We introduce three subduction rates:

Total subduction rate (S_{total}): This is calculated from the 5-day mean data.

Mean subduction rate (S_{mean}): This is calculated from the monthly mean data.

Eddy subduction rate (S_{eddy}): This is defined by the difference between the total and mean (i.e., $S_{eddy} = S_{total} - S_{mean}$) (Nishikawa et al., 2010).

We use the geometry of the velocity vectors to detect eddy (Nencioli et al., 2010). The eddy velocity field has a distinct feature: the velocity of the eddy center is the local smallest; the tangential velocity increases with the distance from the center and reaches a maximum at the edge of eddy. Six constraints were derived based on these characteristics:

i Along an east-west section, υ has to reverse in sign across the eddy center and its magnitude has to increase with distance from the center.

Table 1
The Numbers of Anticyclones and Cyclones Used by the Eddy Synthesis

		Anticyclonic eddies	Cyclonic eddies
Winter	In the whole study region without vorticity limit (Figures 4, 5)	21,179	23,064
	In significant positive correlation value region (Figure 3)	7,812	8,704
	In significant negative correlation value region (Figure 3)	4,631	5,069
	In the whole study region with strong-vorticity (Figure 6)	4,235	4,612
	In the whole study region with weak-vorticity (Figure 6)	4,235	4,612
Summer	No lifetimes limit (Figures 11 and 12)	14,837	10,857
	Lifetimes > 1 day (Figure 15)	6,924	4,432

ii Along a north-south section, u has to reverse in sign across the eddy center and its magnitude has to increase away from it: the sense of rotation has to be the same as for v.
iii Velocity magnitude has a local minimum at the eddy center.
iv The directions of the velocity vectors have to change with a constant sense of rotation around the eddy center and the directions of two neighboring velocity vectors have to lay within the same or two adjacent quadrants (the four quadrants are defined by the north-south and west-east axes: The first quadrant encompasses all the directions from east to north, the second quadrant encompasses the directions from north to west, the third quadrant encompasses the directions from west to south, and the fourth quadrant encompasses the directions from south to east.
v If there are two centers detected by above constrains in the two adjacent grids (about 50 km between them), the position with a larger velocity has to be ignored, and the other is the center of the eddy.
vi The position of the maximum tangential velocity is discriminated in eight directions, and the distance from the position to the eddy center is regarded as the eddy radius in this direction, and the maximum of these radii has to be more than 50 km, otherwise this sample cannot be considered as an eddy.

The grids satisfying the above six conditions are automatically determined as the center of the eddy and the corresponding radius. We found that considering only one component of u/v in four directions (north, south, west, and east) would make the determined radius smaller than the actual radius. In order to improve the method, we used the current velocity to determine radii in four directions.

In order to find out the distribution of SLPVW volume in the eddy, we use a dynamic composite method which tracks the eddy center, the formula is as follows:

$$\overline{E}(x,y) = \frac{1}{N}\int_1^T \sum_{i=1}^{n(t)} E(t,i,x,y)dt \tag{4}$$

$E(t,i,x,y)$ is the physical field of the ith eddy at day t, (x, y) is the horizontal grid index, n is the number of eddy samples per day, T is total number of days, and N is the total sample size ($N = \sum_{t=1}^{T} n(t)$), $\overline{E}(x,y)$ is the sample mean. Table 1 shows the numbers of anticyclones and cyclones used by the eddy synthesis.

3. Different States of the North Pacific SLPVW Between Winter and Summer

3.1. The Mean Distribution of SLPVW and EKE

To illustrate the link between mesoscale oceanic eddies and SLPVW, we draw the mean distribution of SLPVW and EKE in winter (February and March; Figure 1a) and summer (June–August; Figure 1b) over North Pacific. EKE is one of the important physical quantities to quantitatively measure the intensity of eddy activity, it is defined by

$$EKE = \left(\overline{u'^2} + \overline{v'^2}\right)/2 \tag{5}$$

where u and v are zonal and meridional velocities, $u' = u - \overline{u}, v' = v - \overline{v}$, and the bar denotes time mean.

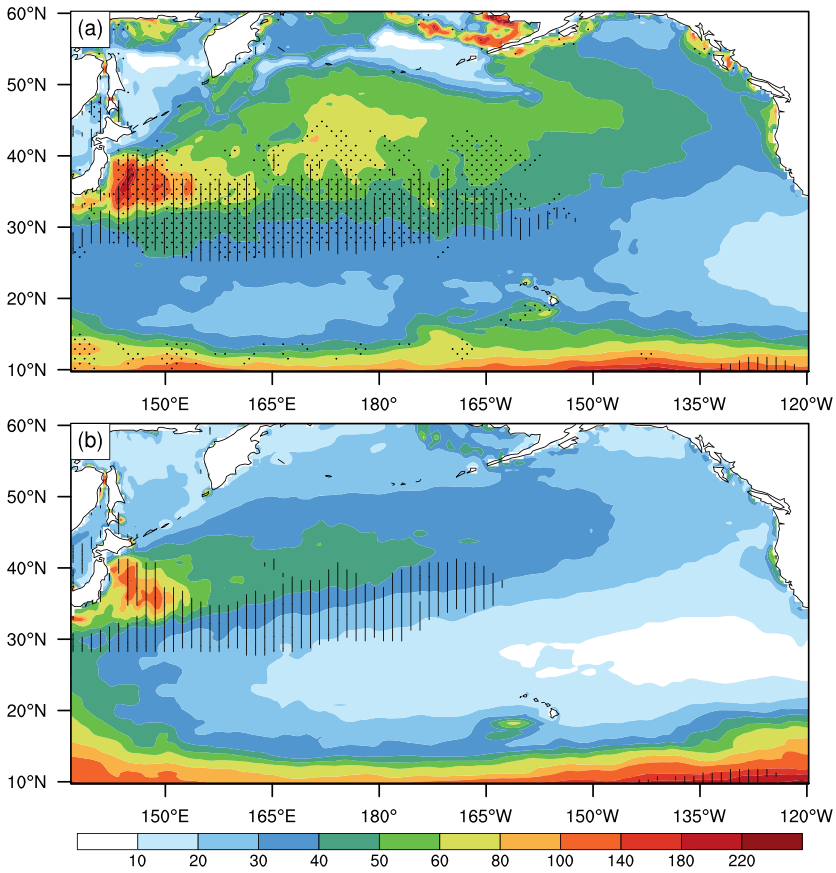

Figure 1. The distribution of EKE (color shade in cm^2/s^2) in (a) winter (February and March) and (b) summer (June–August) from the year 1979 to 2010. The area where the climatic mean thickness of SLPVW is greater than 10 m is covered with vertical lines. The area with large instantaneous subduction rate is covered with dots

EKE reflects the intensity of the eddy activity, and eddies are active in the region of large EKE. In Figure 1, The area where the climatic mean thickness of SLPVW is greater than 10 m (covered with vertical lines) and the region of large EKE mostly coincide, indicating that the mode water is bound to be affected by eddies in winter and summer. The SLPVW is generated and subducted in February and March per year. During this period, the volume of mode water gradually increases; finally, it reaches the maximum value in the early spring and then gradually dissipates. In summer (Figure 1b), the region where the climatic mean thickness of SLPVW is greater than 10 m is smaller than in winter (Figure 1a) and so does EKE. The area where the instantaneous subduction rate is greater than 5×10^{-6} m/s (the dotted area in Figure 1a) is mainly distributed north of 25°N where EKE is large, that implying the contribution of eddy to the instantaneous subduction rate.

3.2. The Distribution of Correlation Coefficient Between SSH and SLPVW

SSH is remarkably negatively correlated with the vorticity in the study region (Figures 2a and 2b), it means SSH can represent eddies to some extent. How does the mesoscale oceanic eddy affect the SLPVW? If there is a seasonal difference in this effect? And whether there is a significant correlation between the SSH affected by mesoscale oceanic eddy and the volume of SLPVW? In order to solve this series of questions, the distribution of correlation coefficient between SSH and SLPVW is displayed from the year 1979 to 2010 separately in winter and summer. It is found that the correlation coefficient between the SSH and the volume of SLPVW in winter (February and March; Figure 2c) is positive in the north of 30°N and negative in the south of 30°N. The sea surface height anomaly (SSHA) is positive in the anticyclone; therefore, the correlation suggests that more SLPVW tends to exist in the anticyclone in the north of 30°N, and less SLPVW tends to exist in the

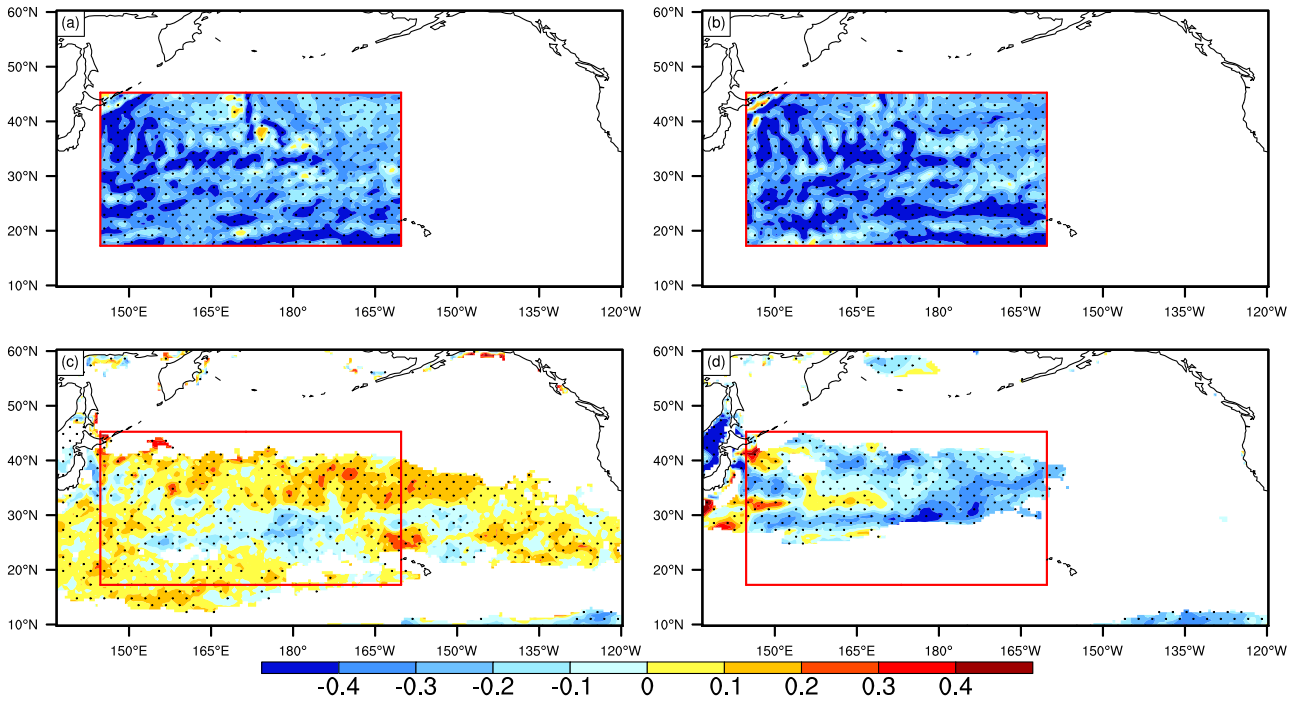

Figure 2. The distribution of correlation coefficient between daily SSH and vorticity in (a) winter (February and March) and (b) summer (June–August) from the year 1979 to 2010. And the correlation coefficient between daily SSH and SLPVW in (c) winter (February and Mar) and (d) summer (June–August) from the year 1979 to 2010. The area passed the 90% significance of *t* test is covered with dots. The area where the climatic mean thickness of SLPVW is greater than 2 m and is filled with colors in (c) and (d).

anticyclone in the south of 30°N. The distribution of correlation in summer (June–August; Figure 2d) is quite different from that in winter, the correlation coefficient is mostly negative. Therefore, less SLPVW tends to exist in the anticyclone. In order to verify this suggestion, we compose winter and summer eddies separately in the study area (marked by the red rectangle frame in Figure 2), then discuss the results of the composition.

4. Compose Eddies and Describe the Mechanism That Eddies Impact on SLPVW in Winter

4.1. The Effect of Eddy on SLPVW in Winter

Considering the correlation between the SSH and the volume of SLPVW in winter is positive in the north of 30°N and negative in the south of 30°N, we compose eddies in remarkably positive and negative correlation value region separately (the entire composite region where thick SLPVW generated is marked by the red rectangle frame in Figure 2). The composition results (Figure 3) reflect the immediate effect of eddies on the SLPVW volume anomaly. In the center of composite anticyclone of the positive correlation value region, the volume of SLPVW increases abnormally, and the greatest increase occurs in the northwest side of the composite anticyclone (Figure 3b); in the center of composite cyclone of the positive correlation value region, the volume of SLPVW decreases abnormally, and the greatest reduction occurs in the west side of the composite cyclone (Figure 3b2). It seems that the MLD anomaly mostly has good correspondence with the SLPVW volume anomaly in composite fields, deepening (shallowing) of the MLD corresponds to the decrease (increase) of the volume of SLPVW. This correspondence exists in both the positive and negative correlation value regions (Figures 3a1 and 3b1, 3a2 and 3b2, 3a3 and 3b3, and 3a4 and 3b4). The positive temperature anomaly of anticyclone decreases with the deepening of depth (Figures 4a–4c), which is conducive to strengthen the ocean stratification, accordingly it may be the cause of the instantaneous shallowing of MLD in the composite anticyclone when the turbulent heat flux (THF) anomaly is not very large. On the contrary, the negative temperature anomaly of cyclone decreases with the deepening of depth

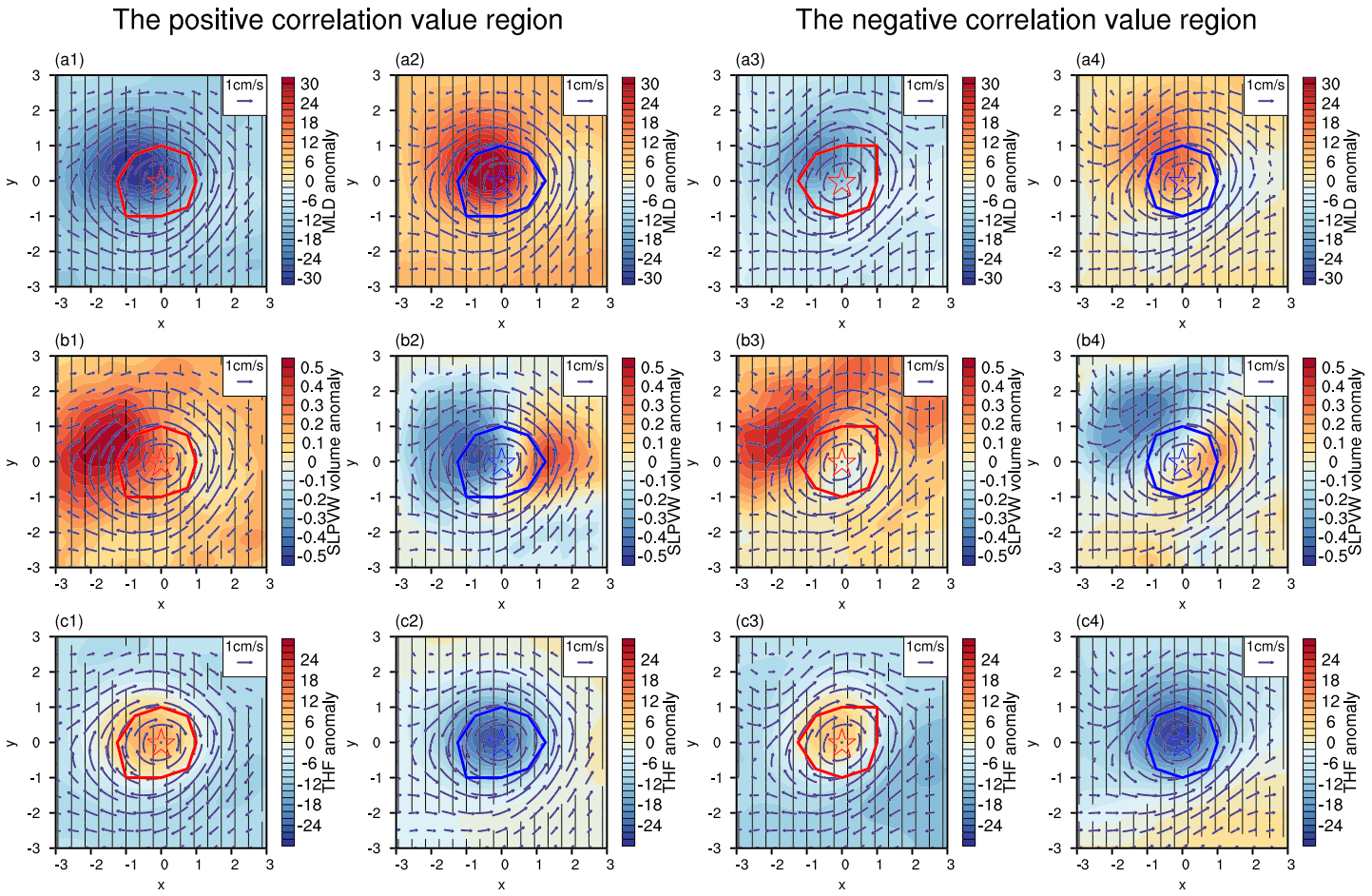

Figure 3. The composite anticyclone (cyclone) in winter from the year 1979 to 2010: (1 and 2 columns) the composite anticyclone and cyclone of the positive correlation value region, (3 and 4 columns) the composite anticyclone and cyclone of the negative correlation value region, (a1–a4) mixed layer depth anomaly (color shade in m), (b1–b4) subsurface low potential vorticity water volume anomaly (color shade in grid points), and (c1–c4) turbulent heat flux anomaly (color shade in W/m^2). The red (blue) asterisk is the center of the composite anticyclone (cyclone), and the red (blue) solid line is the edge of composite anticyclone (cyclone); vector arrows are mean abnormal velocity of flow above 200 m. The area passed the 95% significance of *t* test is covered with vertical lines. Δx and Δy are used relative to the eddy centers, $\Delta x = 1$ means 1° longitude interval, and $\Delta y = 1$ means 1° latitude interval

(Figures 4d–4f), which is conducive to weaken the ocean stratification, and leads to deeper MLD in the composite cyclone when the THF anomaly is not very large. Affected by the vertical decrease of warm advection (Figures 4a–4c), the region where MLD shallows most is in the northwest side of the composite anticyclone (Figures 3a1 and 3a3) and so does the region where low PV water mass under the MLD (namely, SLPVW) increases most (Figures 3b1 and 3b3). And the vertical decrease of cold advection weakens the oceanic stratification in the west side of the composite cyclone (Figures 4d–4f). Therefore, the maximum MLD deepening occurs in the west side of the composite cyclone (Figures 3a2 and 3a4) and so as the maximum decrease of low PV water mass under the MLD (namely, SLPVW) (Figures 3b2 and 3b4).

The composition results in the negative correlation value region are similar to those in the positive correlation value region, but the SLPVW volume decreases abnormally in the center of the composite anticyclone and increases abnormally in the center of the composite cyclone, which is consistent with the weak negative correlation between SSH and the SLPVW volume in the region. The composition results in the negative correlation value region are similar to those in the positive correlation value region after the deflection. What causes the deflective distribution of the composition results? Is it related to the eddy vorticity strength? Next, we will count the distribution of eddy vorticity strength in the whole study area and compose strong vorticity eddies and weak vorticity eddies separately.

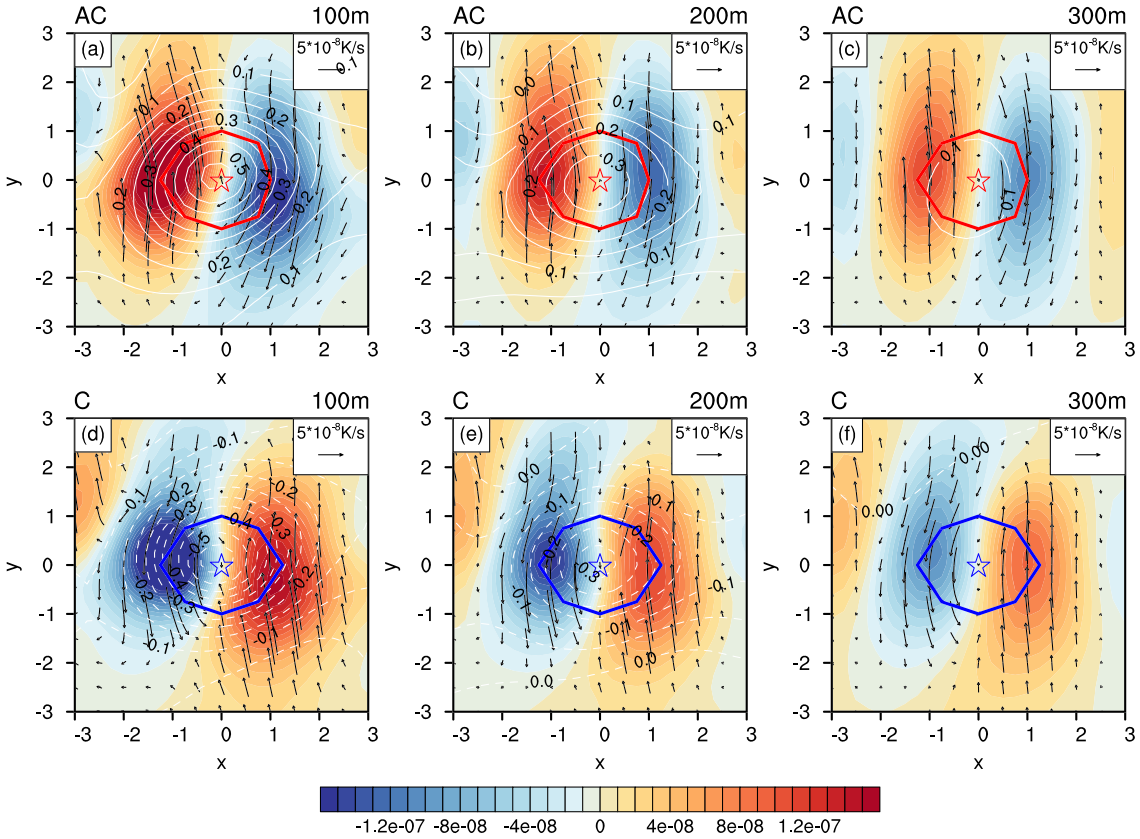

Figure 4. The anomalous temperature (contours; K) the corresponding anomalous temperature advection (adv = $-(u_a \frac{\partial T}{\partial x} + v_a \frac{\partial T}{\partial y})$, shadings; K/s) at different depths (100, 200, and 300 m) in composite fields of all anticyclones (a–c) and cyclones (d–f) in the study region in winter from 1979 to 2010. The contour interval is 0.1 K. The red (blue) asterisk is the center of the composite anticyclone (cyclone), and the red (blue) solid line is the edge of composite anticyclone (cyclone); vector arrows are anomalous temperature advection vectors

4.2. The Distribution of Eddy Vorticity Strength and Strong (Weak) Vorticity Eddies Composition Analysis

The vorticity is remarkably negatively correlated with SSH and SST in the study region (Figures 2a and 2b); it means that the vorticity can represent eddies to some extent. The strength of the eddy can be characterized by the vorticity of the eddy center, and the larger the absolute value of the vorticity, the stronger the eddy is. The number of anticyclones in the positive correlation value region is larger than that in the negative correlation value region (Figure 5) and so does the number of cyclones, which may be related to the larger EKE in the positive correlation value region (Figure 1). However, the number of eddies is not positively correlated with eddy vorticity strength. The distribution of cyclone (anticyclone) vorticity strength in the positive correlation value region shows unimodal characteristic, while in the negative correlation value region the distribution of eddy vorticity strength shows bimodal characteristic. The ratio of the strong eddy in negative correlation value region is significantly larger than that in the positive correlation value region.

In order to verify that the eddy vorticity strength is the main cause of the north-south opposite distribution of the correlation coefficient, we define the eddy with the vorticity in top 20 (bottom 20) percent in the study region is strong-vorticity (weak vorticity) eddy. There are 21,179 anticyclones and 23,064 cyclones in the study region in winter without vorticity limit (Table 1). According to the eddy vorticity in the study region in winter, we finally select and compose the strong eddy that the vorticity of anticyclone (cyclone) center is less (greater) than $-8.675{\cdot}10^{-7}$ s^{-1} ($8.226{\cdot}10^{-7}$ s^{-1}) (4,235 anticyclones and 4,612 cyclones), and the vorticity of anticyclone (cyclone) center is greater (less) than $-2.797{\cdot}10^{-7}$ s^{-1} ($2.7{\cdot}10^{-7}$ s^{-1}) (4,235 anticyclones and 4,612 cyclones), the results are shown in Figure 6. The composition results of the weak eddy (Figures 6a1, 6a2, 6b1, 6b2, 6c1, and 6c2) are similar to those of the positive correlation value region (Figures 3a1,

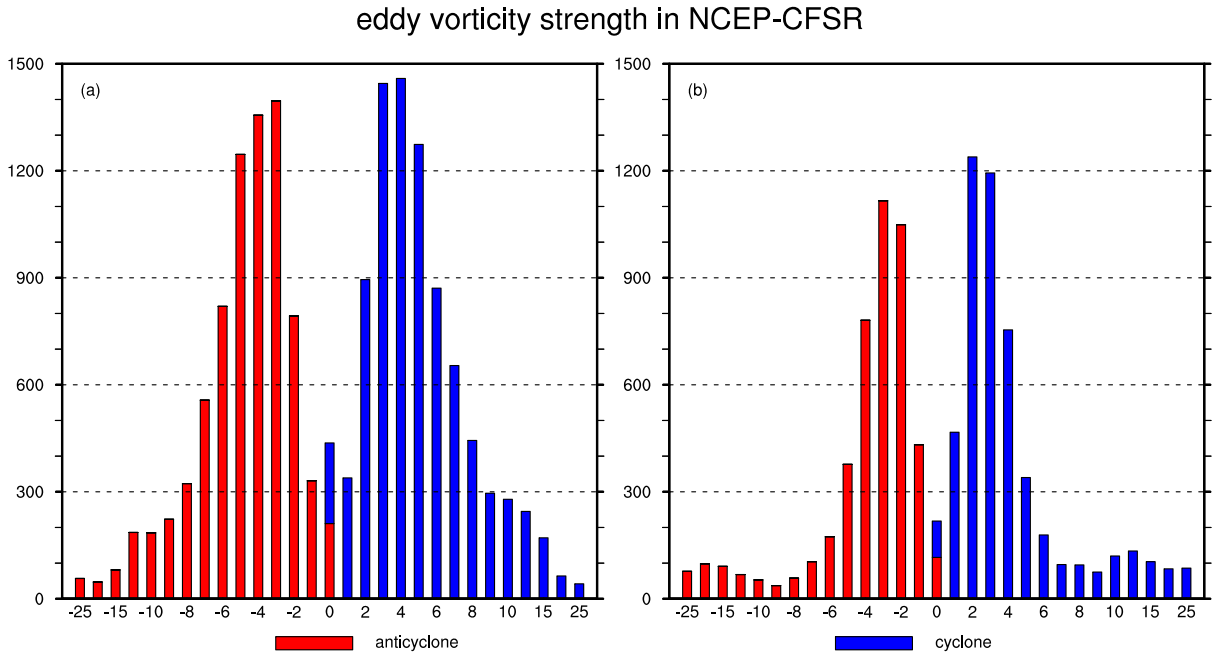

Figure 5. The distribution of eddy vorticity strength (10^{-7} s^{-1}): (a) positive correlation value region and (b) negative correlation value region.

3a2, 3b1, 3b2, 3c1, and 3c2). The abnormal THF of the composite weak eddy is quite different with the composite strong eddy. In the atmosphere above composite weak anticyclone, temperature anomaly at 2-m above sea surface is very large. In the meantime, SSTA is much smaller than it. Weak anticyclone may be the decay stage of the preexisting strong anticyclone. The distance of the motion of the eddies is far less than the radius of the eddies. In the early stage, strong anticyclone has been heating the atmosphere, and the large heat loss weakens anticyclone itself. Then it becomes the weak anticyclone in the decay period. At this time, the local temperature difference between the ocean and atmosphere is much smaller than before (Figures 6d1 and 6e1) and so does the local wind speed (Figure 6f1); therefore, the abnormal THF is negative in the composite weak anticyclone. The warm characteristics of the weak anticyclone and the negative abnormal THF together, all these factors have resulted in shallower MLD in the weak anticyclones and caused by warm advection MLD shallows most in the northwest side of the composite weak anticyclone (Figure 6a1). On the contrary, due to the cool characteristics of the weak cyclone, MLD tends to be deeper and caused by cold advection MLD deepens most in the northwest side of the composite weak cyclone (Figure 6a2).

The composition results of the strong eddy (Figures 6a3, 6a4, 6b3, 6b4, 6c3, and 6c4) are similar to those in the negative correlation value region (Figures 3a3, 3a4, 3b3, 3b4, 3c3, and 3c4). The SLPVW volume is abnormally decreased in the center of the composite anticyclone, and abnormally increased in the center of the composite cyclone, but the distribution of extreme value is a bit different. As we can see, there is a weaker eddy in the west-northwest side of the main eddy, which rotating reversely, and this coexistence of two eddies may be the cause of the shift of the extreme value distribution. The abnormal THF of strong eddy (Figures 6c3 and 6c4) is much stronger than usual. Therefore, it has a great influence on MLD. The large abnormal THF (more heat loss than usual) of the strong anticyclone (Figure 6d3) can induce deep convection which is beneficial to generate thicker ML (namely, deeper MLD) (Figure 6a3). Although the deeper MLD correspond to more low PV water generation, the low PV water mass that actually enters the subsurface ocean below the MLD (namely, SLPVW) is decreased due to the deeper MLD. However, the smaller abnormal THF over the weaker cyclone, which in the west-northwest side of the strong anticyclone, together with the stronger ocean stratification caused by the warm advection, finally cause the decrease of MLD. Since the THF anomaly greatly changes the gradient of MLD anomaly in the composite region, which is beneficial to subduction, a large amount of SLPVW generates in the west side of the strong anticyclone.

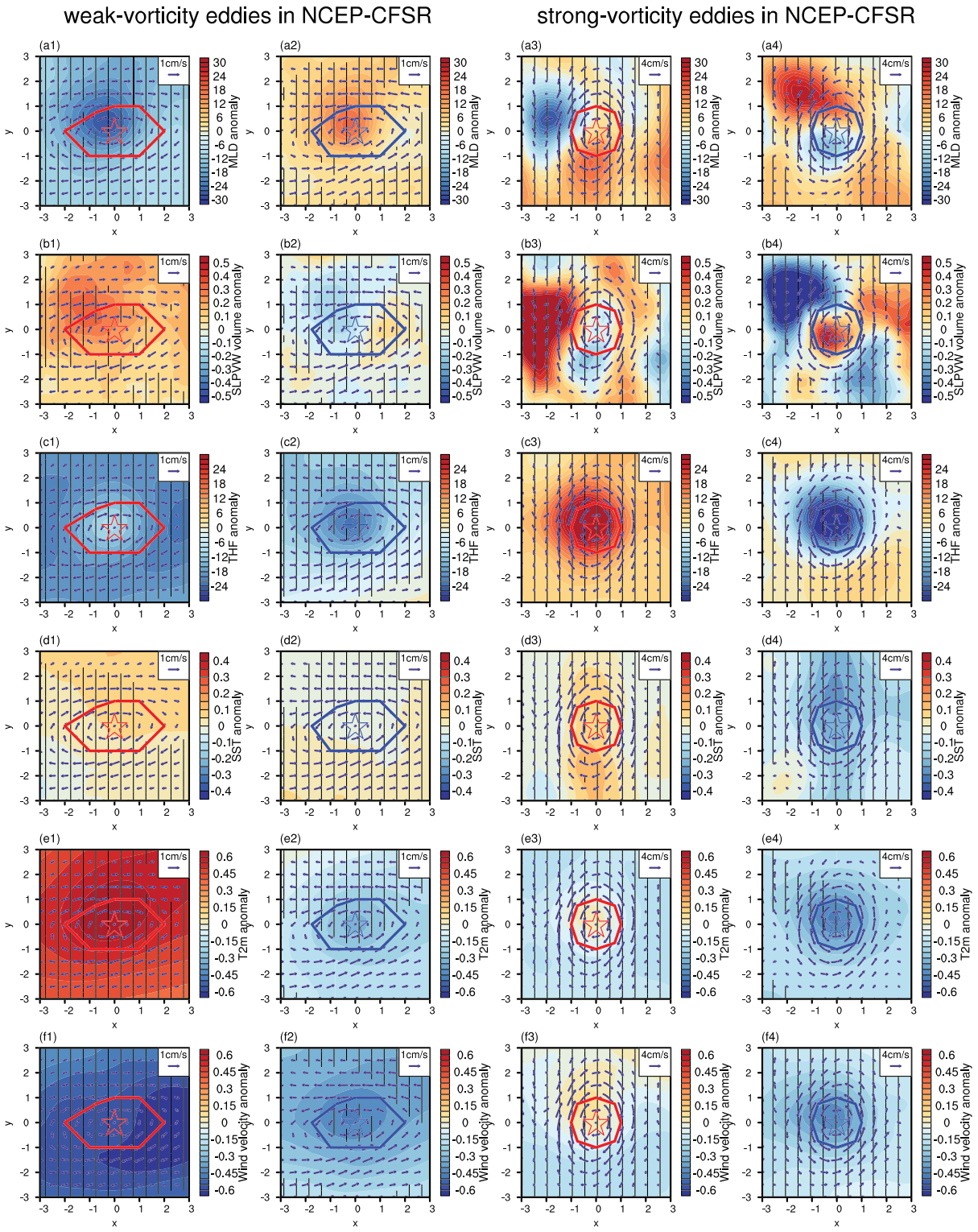

Figure 6. The composite anticyclone (cyclone) in winter from the year 1979 to 2010: (1 and 2 columns) the composite anticyclone and cyclone of the weak-vorticity eddies and (3 and 4 columns) the composite anticyclone and cyclone of the strong-vorticity eddies. The area passed the 95% significance of *t* test is covered with vertical lines: (a1–a4) mixed layer depth anomaly (color shade in m), (b1-–4) subsurface low potential vorticity water volume anomaly (color shade in grid points), (c1–c4) turbulent heat flux anomaly (color shade in W/m^2), (d1–d4) sea surface temperature anomaly (color shade in °C), (e1–e4) temperature anomaly at 2 m above ground (color shade in °C), and (f1–f4) wind velocity anomaly (color shade in m/s). The red (blue) asterisk is the center of the composite anticyclone (cyclone), and the red (blue) solid line is the edge of composite anticyclone (cyclone), vector arrows are mean abnormal velocity of flow above 200 m. Δx and Δy are used relative to the eddy centers, $\Delta x = 1$ means 1° longitude interval, and $\Delta y = 1$ means 1° latitude interval.

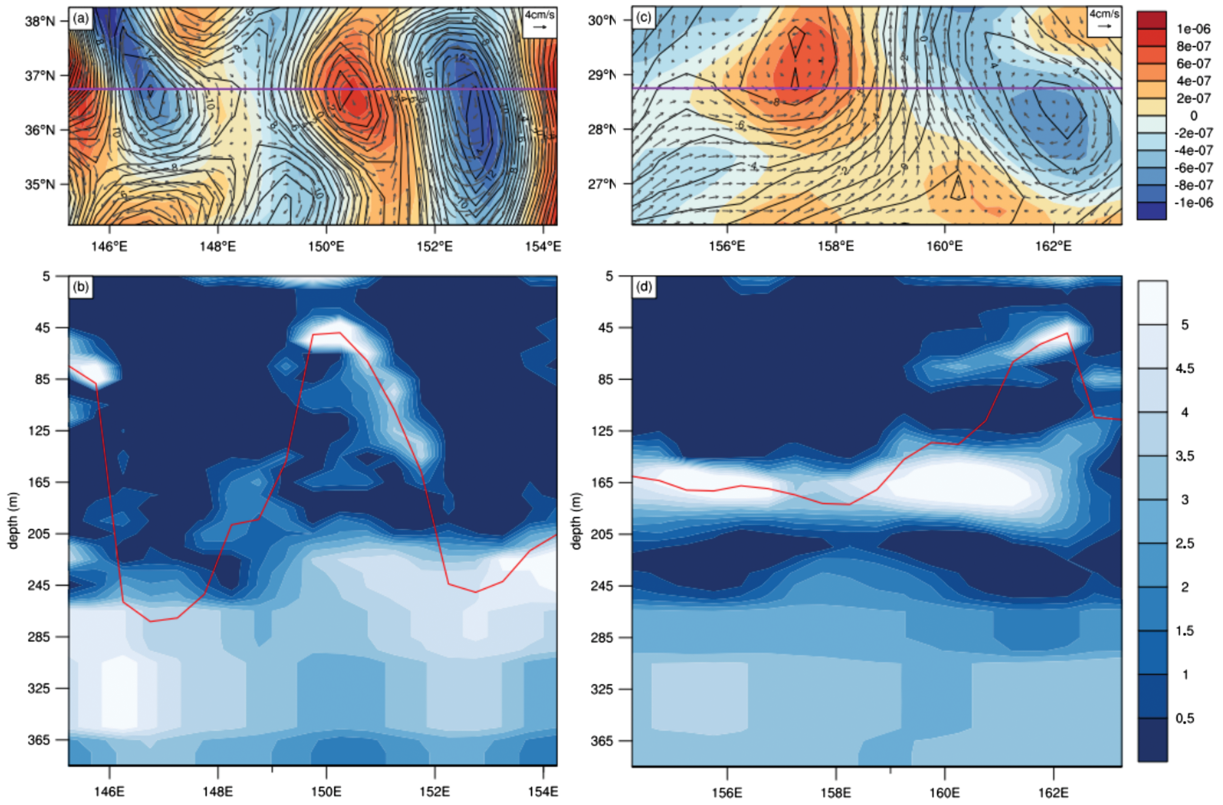

Figure 7. (a) The distribution of vorticity (color shade in s^{-1}) and SSHA (black contours in cm) in 34.25°N–38.75°N, 145.25°E–154.25°E on 23 March 1981; (b) The section across 36.75°N, where marked by purple solid line in the (a), shows the distribution of potential vorticity (PV; color shade in 10^{-10} m^{-1} s^{-1}); the solid red line is MLD (m). (c) The distribution of vorticity (color shade in s^{-1}) and SSHA (black contours in cm) in 26.25°N–30.25°N, 154.25°E–163.75°E on 20 March 2007; (d) The section across 28.75°N, where marked by purple solid line in the (c), shows the distribution of potential vorticity (PV; color shade in 10^{-10} m^{-1} s^{-1}); the solid red line is MLD (m).

Figure 7a shows the distribution of vorticity and SSHA in the region of 34.25°N–38.75°N, 145.25°E–154.25°E on 23 March 1981. The 36.75°N latitude line passes through a strong anticyclone, a strong cyclone, and another strong anticyclone from west to east, and Figure 7b shows the distribution of PV and MLD in the section along 36.75°N. The MLD in the strong anticyclone is deep, and there is a large amount of low PV water in the ML. On the contrary, the MLD in the strong cyclone is much shallower, and there is more low PV water under the MLD (namely, SLPVW), although less low PV water generated in ML. The difference of the MLD between strong anticyclone and strong cyclone is more than 200 m, and the great horizontal gradient of the MLD between anticyclone and cyclone is conducive to the subduction. Figure 7c shows the distribution of vorticity and SSHA in the region of 26.25°N–30.25°N, 154.25°E–163.75°E on 20 March 2007. The 28.75°N latitude line passes through a weak cyclone and a weak anticyclone from west to east, and Figure 7d shows the distribution of PV and MLD in the section along 28.75°N. The MLD in the weak cyclone is deep, and there is a large amount of low PV water in the ML. On the contrary, the MLD in the weak anticyclone is much shallower, and there is more low PV water under the MLD (namely, SLPVW), although less low PV water generated in ML. The difference of the MLD between weak anticyclone and weak cyclone is about 100 m, and the horizontal gradient of the MLD between weak anticyclone and weak cyclone is far less than that between strong anticyclone and strong cyclone.

Based on the composition results and the above cases, the schematic view of the influence of weak and strong eddies on SLPVW generation process in winter is given (Figure 8). The relationship between winter oceanic eddies and SLPVW volume is influenced by the eddy vorticity strength. The THF anomaly of the weak-vorticity eddy is much smaller than usual; the vertical distribution of temperature anomaly seems to play a more important role in the SLPVW generation process. The positive temperature anomaly of anticyclone (cyclone) decreases (increases) with the deepening of depth, which is conducive to strengthen

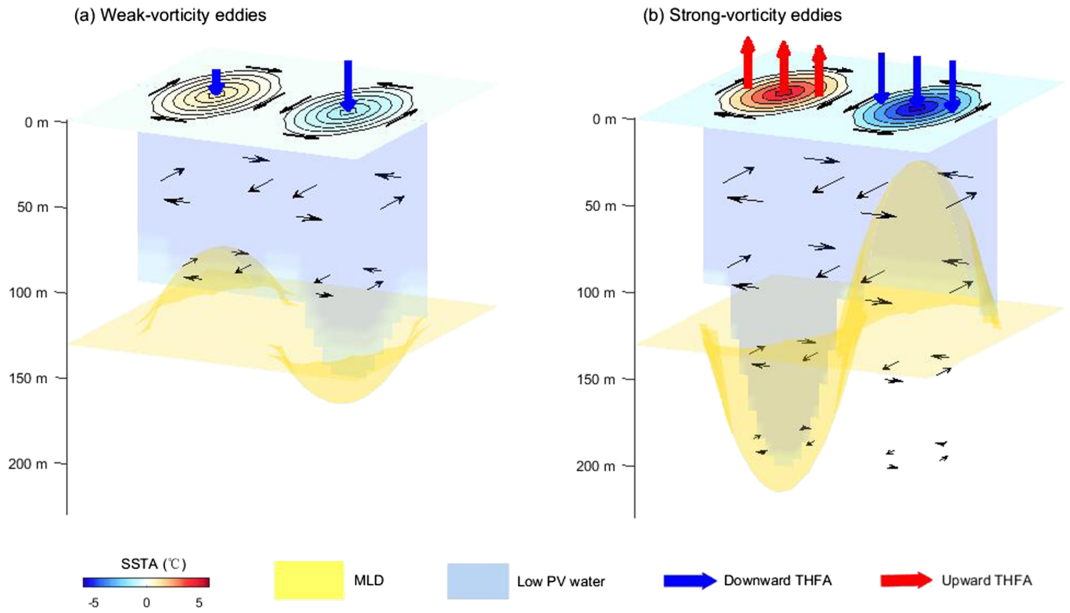

Figure 8. The schematic view of (a) strong-vorticity eddies and (b) weak-vorticity eddies in winter.

(weaken) the ocean stratification, causes the shallower (deeper) MLD and less (more) low PV water, but leads to the increasing (decreasing) of the low PV water mass under MLD (namely SLPVW) (Figure 8a). The THF anomaly of the strong-vorticity eddy is much stronger than weak eddy, which can lead to great change on MLD. The large positive THF anomaly (more heat loss than usual) of the strong-vorticity anticyclone can induce deep convection which is beneficial to generate thicker ML (namely, deeper MLD), which leads to the increasing of the low PV water mass, but decreasing of the low PV water mass under MLD (namely, SLPVW). And the large negative THF anomaly of the strong-vorticity cyclone can restrain convection, which leads to shallower MLD, finally causes the increasing of SLPVW (Figure 8b). Moreover, considering that the horizontal resolution of NCEP-CFSR data may be questioned whether it is enough to catch the detail structures of each eddy. To make the conclusions concerning oceanic eddies more convincing, we add analyses of HYCOM/NCODA data in the discussion (section 6) to confirm the results shown in the present section.

4.3. The Effect of Winter Eddies on Subduction Rate

The results of the above composite analysis reflect the immediate effect of eddies on MLD, SLPVW, and turbulent heat flux. In addition, eddies also contribute to the subduction rate. Nishikawa et al. (2010) pointed out that the contribution by mesoscale oceanic eddies accounts for about 50% of the total subduction rate. To examine the role of mesoscale oceanic eddies in subduction, we introduce three subduction rates: total subduction rate (S_{total}), mean subduction rate (S_{mean}), and eddy subduction rate (S_{eddy}). The calculation methods are described in section 2. Obviously, the total subduction rate varies greatly from year to year, and it has a big difference with the mean subduction rate (Figure 9a), suggesting the role of the interannual variation of eddies on the subduction rate. From 1979 to 2010, the time-averaged total subduction rate of NP (the region marked by red rectangle frame in Figure 2) is 5.15 Sv in the NCEP-CFSR, and the time-averaged eddy subduction rate is 1.88 Sv, accounting for 36.4% of the time-averaged total subduction rate.

In 1999, 2002, 2009, and 2010, the mean subduction rate was negative (Figure 9a); it may be caused by the abnormal horizontal gradient of the ML, which is sensitive to the change of the heat flux. Not every year, the eddy has a positive contribution to the subduction rate. In 1980, 1981, 1984, 1991, and 2004, the eddy subduction rate was negative (Figure 9a), but the time-averaged eddy subduction rate is 1.88 Sv.

The varied contribution of eddies to the subduction rate may be related to the interannual different distributions of cyclones and anticyclones. Figure 9b indicates that both the anticyclone and cyclone have obvious interannual variations. The correlation between the total subduction rate and the number of anticyclones

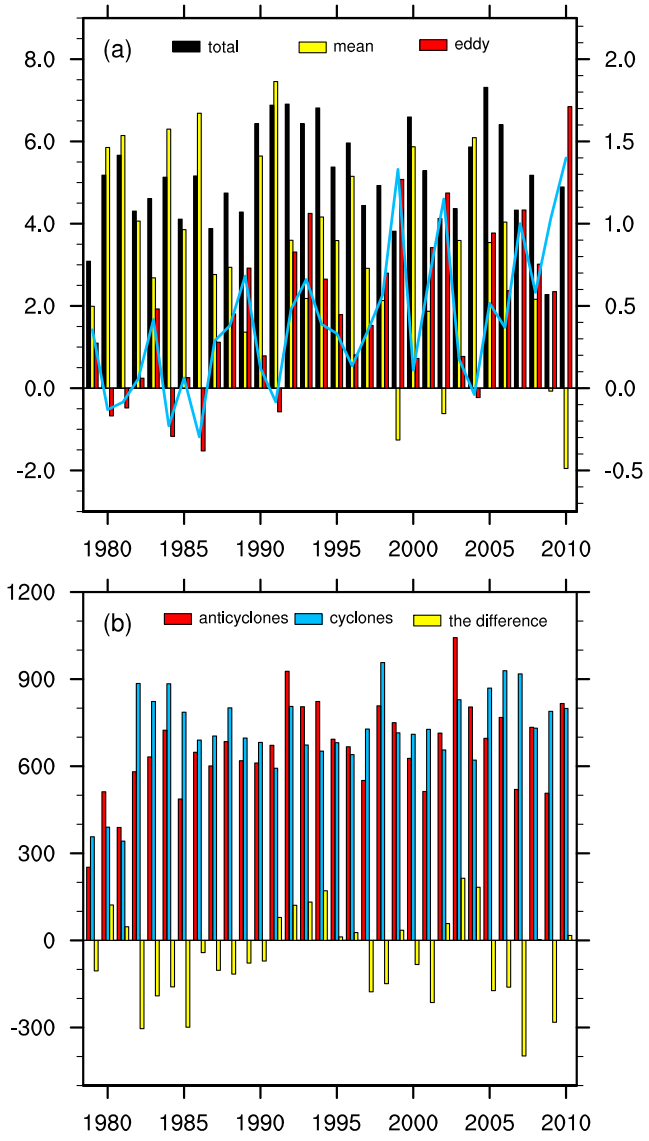

Figure 9. (a) Annual subduction rate (Sv, reference left vertical axis) based on the maximum ML base. The calculation region is denoted by red lines in Figure 2 (black bar: total subduction rate, yellow bar: mean subduction rate, red bar: eddy subduction rate; blue solid line: the radio of eddy subduction rate to total subduction rate, and reference right vertical axis); (b) the annual quantity of eddies, the calculation region is same as (a) (red bar: the number of anticyclones, blue bar: the number of cyclones, and yellow bar: the difference number between anticyclones and cyclones).

in the study region is remarkably positive; the correlation coefficient is 0.40. Similarly, the total subduction rate is positively correlated with the difference of the number of anticyclones and cyclones. The correlation coefficient is 0.40 that passes the 95% significance of t test. The correlation coefficient between the eddy subduction rate and the number of anticyclones fails to the 90% significance of t test. Since the velocity anomaly and the horizontal gradient of MLD anomaly are greater in the strong-vorticity composite eddy than in the weak-vorticity composite eddy (Figure 6), we can infer that the subduction rate is not only affected by the number of eddies but also affected by the intensity of eddies. We use the absolute value of vorticity to represents the intensity of eddies and introduce the composite variable EI which combining the number of eddies and the intensity of eddies; the formula is as follows:

$$EI_{ac}(T) = \sum_{i=1}^{N_{ac}(T)} |Vor_{ac}(i)| \tag{6}$$

$$EI_{c}(T) = \sum_{j=1}^{N_{c}(T)} |Vor_{c}(j)| \tag{7}$$

T is year, $N_{ac}(T)$ ($N_c(T)$) is the number of the anticyclones (cyclones) in winter of year: T.$|Vor_{ac}(i)|$($|Vor_c(j)|$) is the absolute value of vorticity in the center of the ith (jth) anticyclone (cyclone) in winter of year: T. The correlation coefficient between the eddy subduction rate and EI_{ac} in the study region is 0.42 that passes the 95% significance of t test. The eddy subduction rate is positively correlated with the difference of the EI_{ac} and EI_c. The correlation coefficient is 0.45 that passes the 95% significance of t test.

5. Composite Eddies and Describe the Mechanism that Eddies Impact on SLPVW in Summer

5.1. Eddies Composition Analysis and Cases Analysis

In summer, SLPVW usually exists in the depth range of 100–250 m (Figure 10), while the mean MLD is 18.3 m, which is much shallower than winter, and shallower than the SLPVW depth range. Moreover, the summer ML hardly changes, and the seasonal thermocline disconnects the exchange of SLPVW and the upper ocean, so there is no SLPVW newly generated. At this time, the effect of mesoscale oceanic eddies on SLPVW is mainly reflected in the dissipation or retention process. In summer, SSH is remarkably negatively correlated with SLPVW volume (Figure 2d), indicating that SLPVW is less in anticyclones. In order to verify this point, we similarly compose eddies in summer.

The composition results show that the SLPVW volume is abnormally decreased in the center of the composite anticyclone, and abnormally increased in the center of the composite cyclone (Figure 11). To make the conclusions concerning summer oceanic eddies more convincing, we add analyses of HYCOM/NCODA data in the discussion (section 6), and its summer composition results are similar to that using NCEP-CFSR data.

Does this imply that the summer anticyclone accelerates the dissipation of SLPVW? Moreover, we offer the abnormal PV three-dimensional distribution and the distribution of the divergence anomaly in the composite eddies (Figure 12). It is found that the positive anomaly of divergence in the composite anticyclone decreases with depth growing, which leads to compressing of low PV water mass between adjacent isopycnic surfaces. Therefore, the PV value increases anomaly in the composite anticyclone, which accelerated the dissipation of SLPVW. However, the negative anomaly of divergence in the composite cyclone decreases with

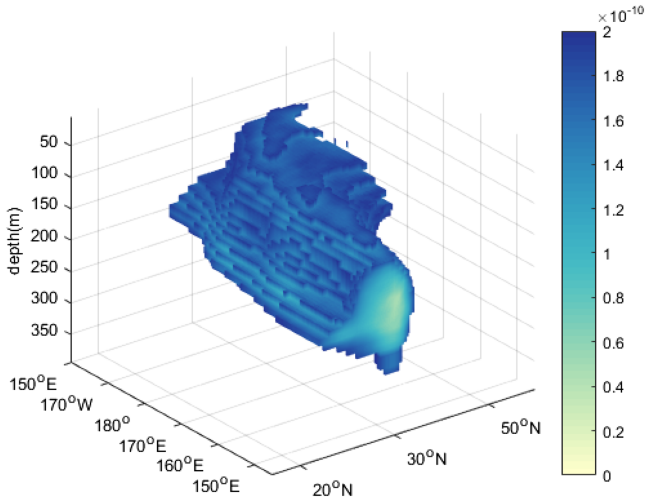

Figure 10. The distributions of the SLPVW in summer (PV; color shade in 10^{-10} m^{-1} s^{-1}).

depth growing, which leads to stretching of low PV water mass between adjacent isopycnic surfaces. Therefore, the PV value decreases anomaly in the composite cyclone, which is beneficial to the retention (or "generation") of the SLPVW. Different from the effect of air-sea heat exchange in winter, in summer, the rotation of the eddies leads to the convergence and divergence, thus changing the stratification of the ocean and ultimately affecting the dissipation of SLPVW. Furthermore, the three-dimensional distribution suggests that the influence of the summer mesoscale oceanic eddies on the PV can reach the depth of 300 m, covering the depth range of the climatological mean SLPVW in summer (100–250 m).

Figure 13a shows the distribution of vorticity and SSHA in the region of 30.75°N–33.75°N, 173.75°E–179.75°E on 20 June 1983. The 32.5°N latitude line passes through an anticyclone, and Figure 13b shows the distribution of PV, potential density and its climatic mean value in the section along 32.5°N. The distance between 25.6 and 25.8 isopycnic surfaces in the range of anticyclone is smaller than the climatic mean state. Figure 13c shows the distribution of vorticity and SSHA in the region of 28.75°N–32.25°N, 177.75°W–172.75°W on 10 June 2010. The 31.25°N latitude line passes through a cyclone, and Figure 13d shows the distribution of PV, potential density, and its climatic mean value in the section along 31.25°N. The distance between 25.8 and 26 isopycnic surfaces in the range of cyclone is larger than the climatic mean state.

Based on the composition results and the above case, the schematic view of the influence of the eddies on SLPVW dissipation process in summer is given (Figure 14). Different from thermodynamic factors impacting the SLPVW generation process in winter, the dynamic factors play a more important role in the SLPVW migration process. Water diverges in the anticyclone, which leads to compressing of low PV water mass between adjacent isopycnic surfaces. Therefore, the PV value increases anomaly in the anticyclone, which accelerated the dissipation of SLPVW. However, water converges in the composite cyclone, which leads to

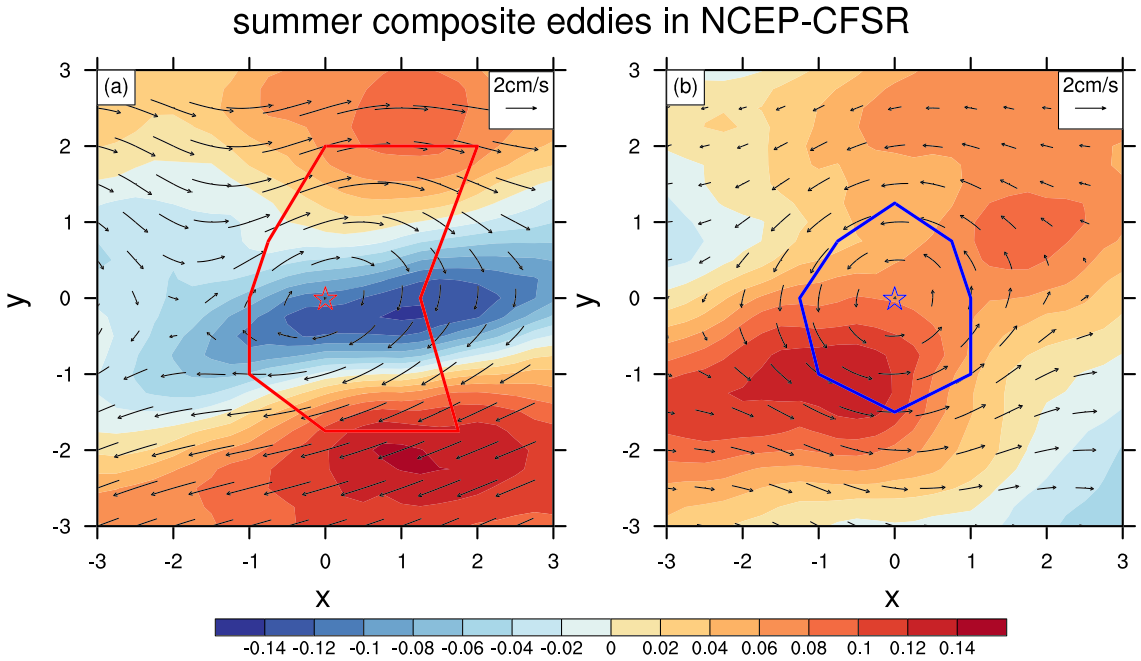

Figure 11. The SLPVW volume anomaly in composite anticyclone (a) and cyclone (b) in summer from the year 1979 to 2010. The red (blue) asterisk is the center of the composite anticyclone (cyclone), and the red (blue) solid line is the edge of composite anticyclone (cyclone); vector arrows are mean abnormal velocity of flow above 200 m. Δx and Δy are used relative to the eddy centers, $\Delta x = 1$ means 1° longitude interval, and $\Delta y = 1$ means 1° latitude interval.

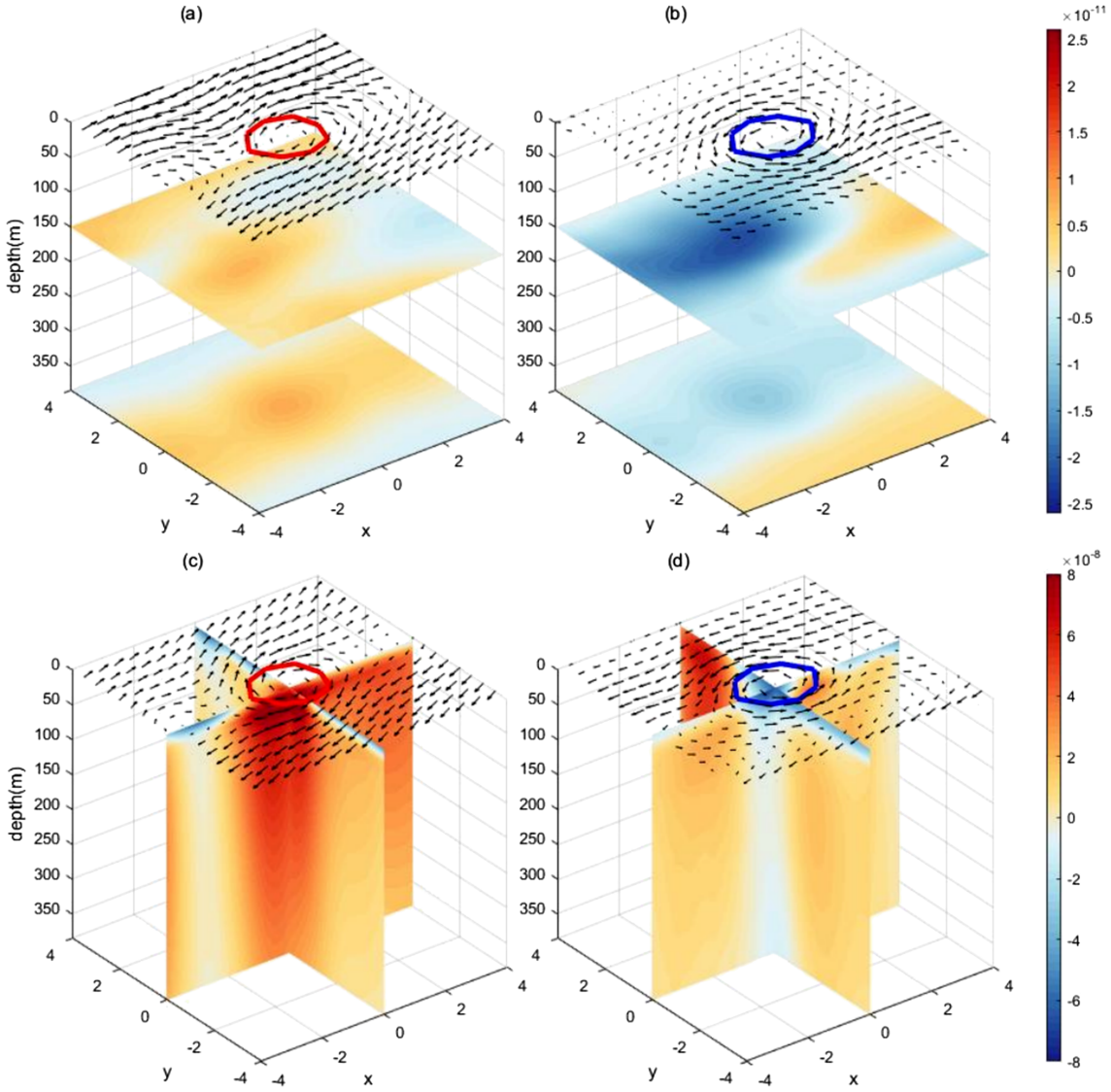

Figure 12. The potential vorticity anomaly (PV; color shade in 10^{-11} m^{-1} s^{-1}) and divergence anomaly (color shade in 10^{-8} s^{-1}) in composite anticyclone (a) and cyclone (b) in summer from the year 1979 to 2010. The red (blue) solid line is the edge of composite anticyclone (cyclone), and vector arrows are mean abnormal velocity of flow above 200 m, the sections based on 150 and 385 m. Δx and Δy are used relative to the eddy centers, $\Delta x = 1$ means 1° longitude interval, and $\Delta y = 1$ means 1° latitude interval.

stretching of low PV water mass between adjacent isopycnic surfaces. Therefore, the PV value decreases anomaly in the composite cyclone, which is beneficial to the retention of the SLPVW.

5.2. Trapped Depth

The volume of SLPVW that can be trapped and transported depends on the ratio of the rotational velocity to migration velocity of the eddy, which is known as the nonlinear constant. This nonlinear constant represents the nonlinearity of the mesoscale oceanic eddy, if the nonlinear constant is greater than 1, the anomalous parameter in the mesoscale oceanic eddy (compared to the surrounding environment) can be well preserved and transported (Flierl, 1981).

After determining the center and boundary of the eddy, we can obtain the migration velocity by tracking of the individual eddy, which can be divided into 5 steps: (i) define the tracking range based on the horizontal resolution of the data set; (ii) assuming that a eddy is found at time t, the same type (cyclonic or anticyclonic) and the nearest eddy are found in the tracking range at time $t + 1$; (iii) if at time $t + 1$, there is no qualified

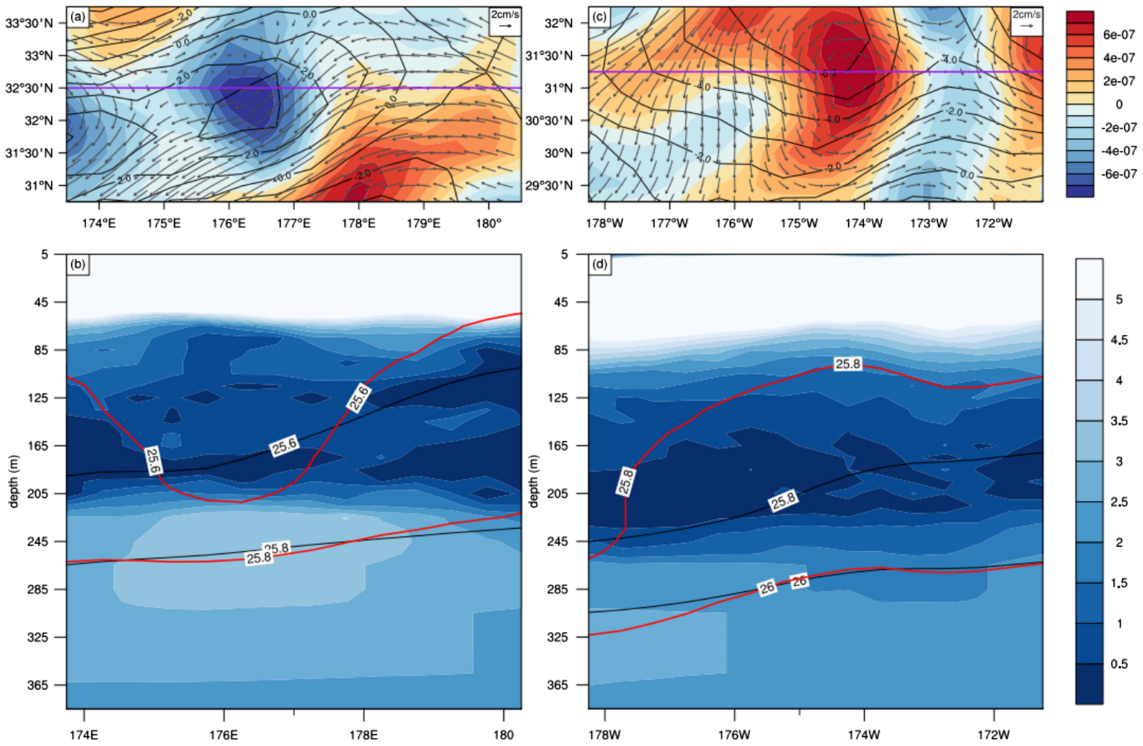

Figure 13. (a) The distribution of vorticity (shadings; 10^{-6} s^{-1}) and SSHA (contours; cm) in 30.75°N–33.75°N, 173.75°E–179.75°E on 20 June 1983; (b) The section across 32.5°N, where marked by purple solid line in the (a), shows the distribution of potential vorticity (shadings; 10^{-10} m^{-1} s^{-1}), the distribution of potential density (red contours; kg/m^3 −1,000) and its climatic mean value (black contours; kg/m^3 −1,000). (c) The distribution of vorticity (shadings; 10^{-6} s^{-1}) and SSHA (contours; cm) in 28.75°N–32.25°N, 177.75°W–172.75°W on 10 June 2010; (d) The section across 31.25°N, where marked by purple solid line in the (c), shows the distribution of potential vorticity (shadings; 10^{-10} m^{-1} s^{-1}), the distribution of potential density (red contours; kg/m^3 −1,000) and its climatic mean value (black contours; kg/m^3 −1,000).

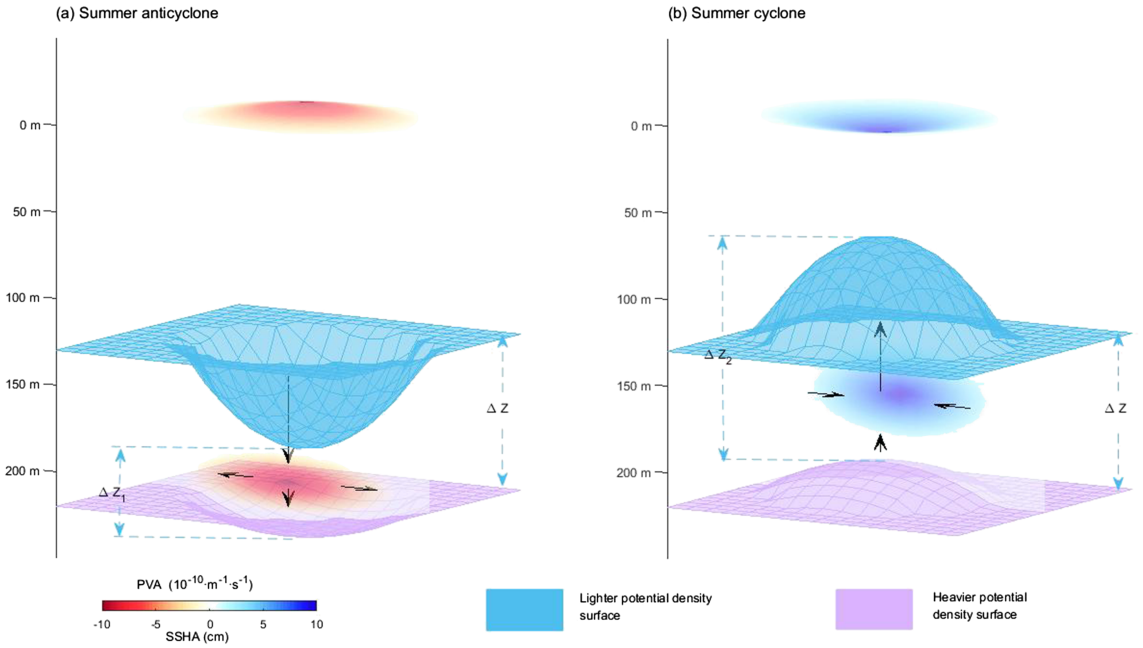

Figure 14. The schematic view of eddies in summer.

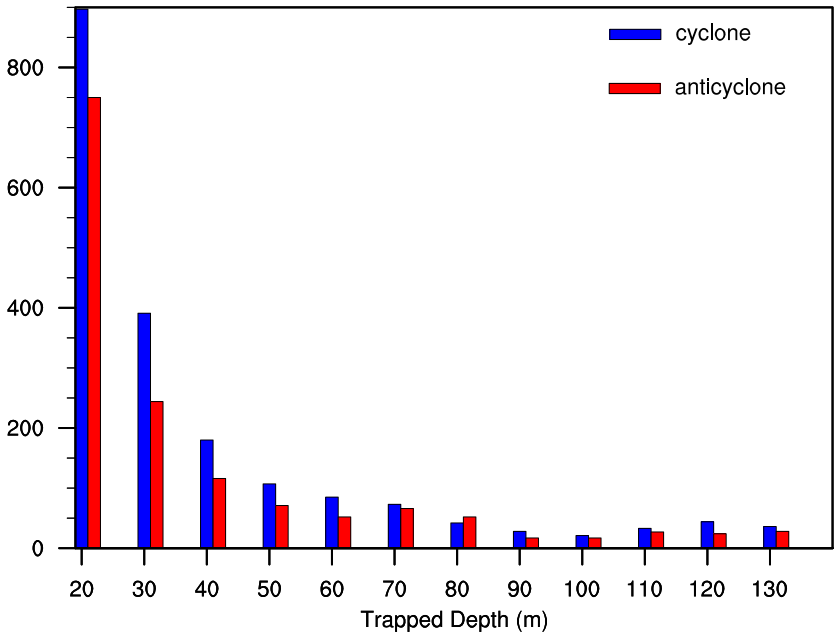

Figure 15. The distribution of trapped depth of anticyclones (red bar) and cyclones (blue bar) in summer from the year 1979 to 2010.

eddy found in the tracking range, it will find the same type of eddy at time $t + 2$ with 1.5 times tracking range, in order to avoid the omission; (iv) if it is still not found, the eddy is considered to last to time t; (v) and if more than one eddy of the same type is found at the same time in the tracking range, take the nearest one

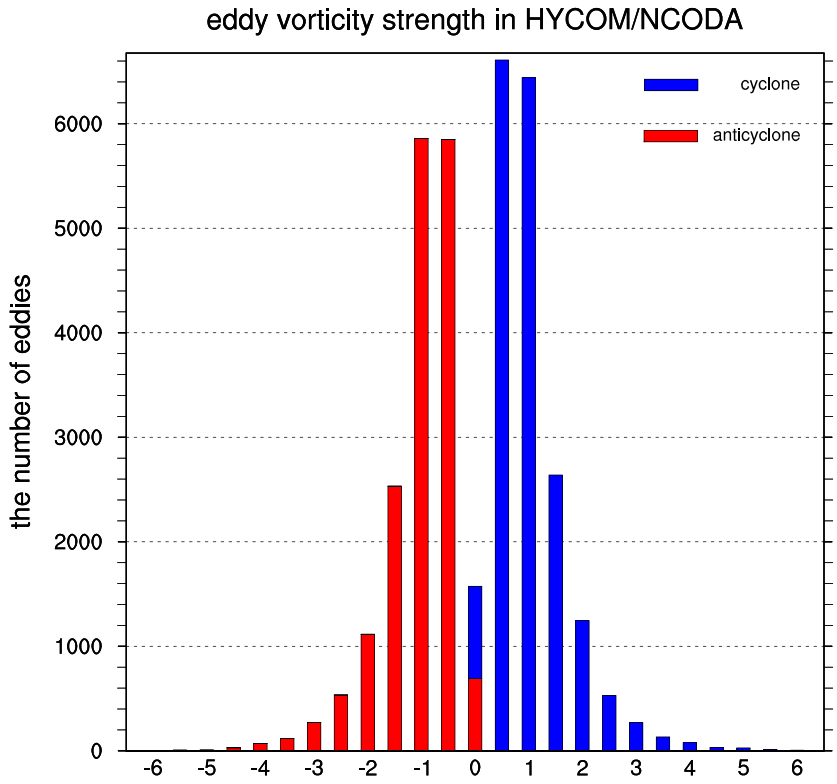

Figure 16. The distribution of eddy vorticity strength (10^{-5} s^{-1}) in HYCOM/NCODA.

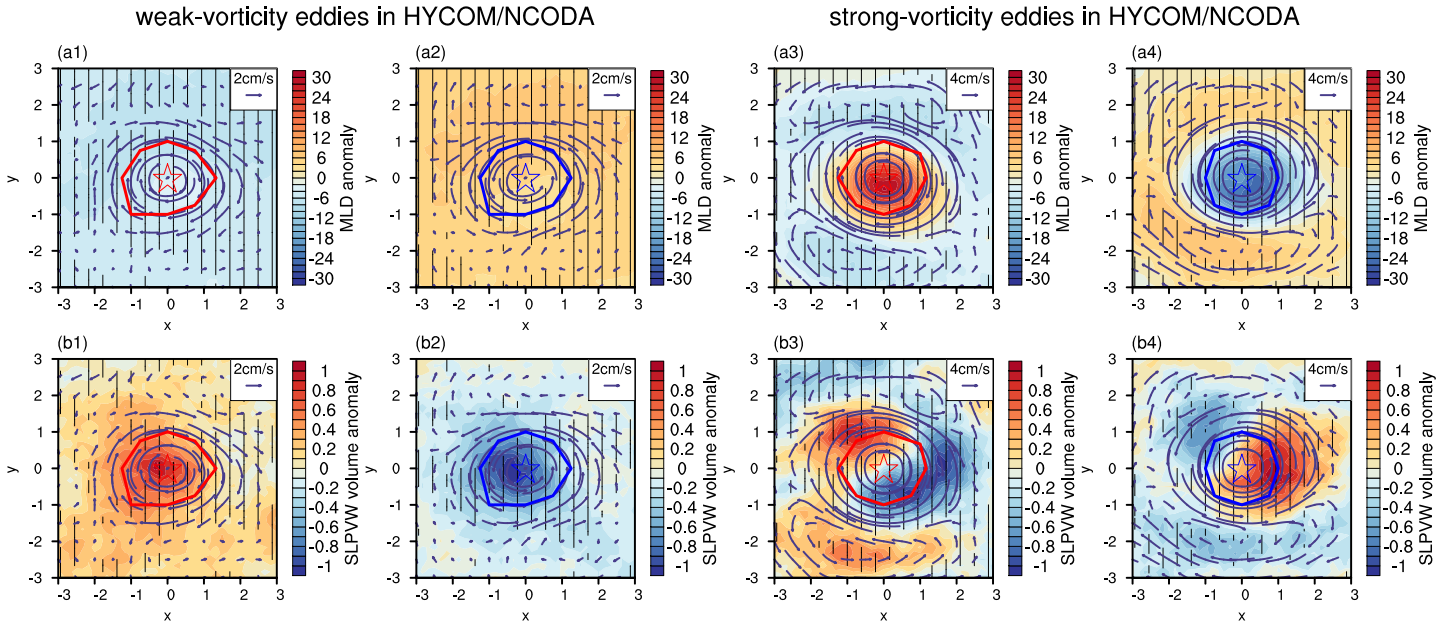

Figure 17. The composite anticyclone (cyclone) in winter from the year 2001 to 2010 in HYCOM/NCODA: (1 and 2 columns) the composite anticyclone and cyclone of the weak-vorticity eddies, (3 and 4 columns) the composite anticyclone and cyclone of the strong-vorticity eddies. The area passed the 95% significance of *t* test is covered with vertical lines: (a1–a4) mixed layer depth anomaly (color shade in m), (b1–b4) subsurface low potential vorticity water volume anomaly (color shade in grid points). The red (blue) asterisk is the center of the composite anticyclone (cyclone), and the red (blue) solid line is the edge of composite anticyclone (cyclone); vector arrows are mean abnormal velocity of flow above 200 m. Δx and Δy are used relative to the eddy centers, $\Delta x = 1$ means 1° longitude interval, and $\Delta y = 1$ means 1° latitude interval.

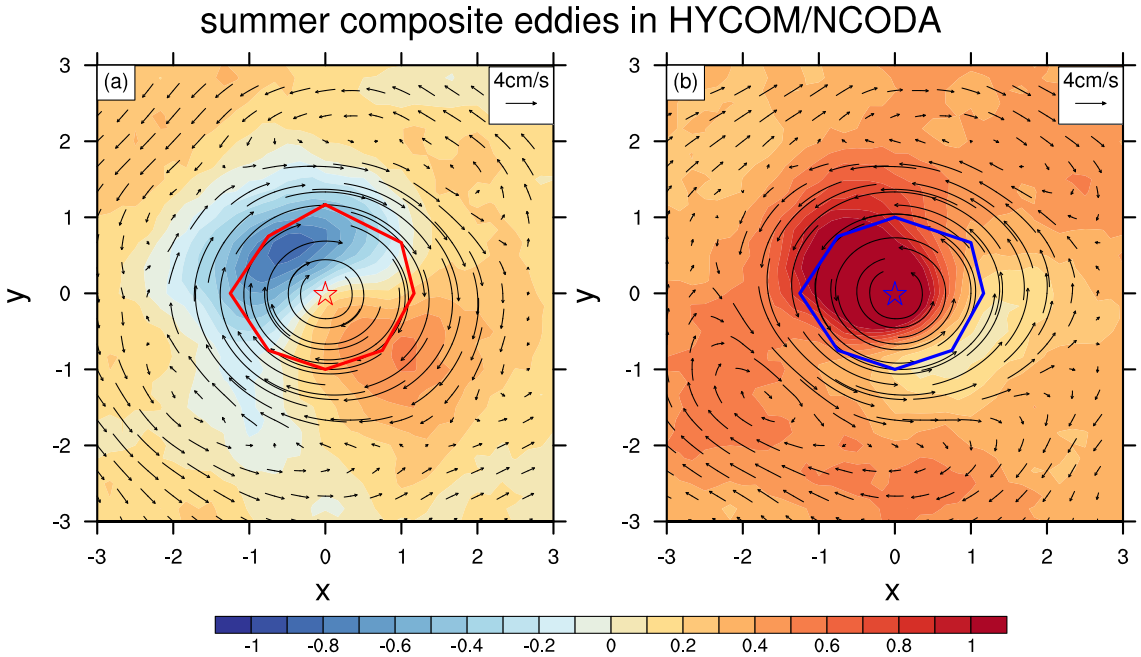

Figure 18. The SLPVW volume anomaly in composite anticyclone (a) and cyclone (b) in summer from the year 2001 to 2010 in HYCOM/NCODA. The red (blue) asterisk is the center of the composite anticyclone (cyclone), and the red (blue) solid line is the edge of composite anticyclone (cyclone); vector arrows are mean abnormal velocity of flow above 200 m. Δx and Δy are used relative to the eddy centers, $\Delta x = 1$ means 1° longitude interval, and $\Delta y = 1$ means 1° latitude interval.

from the eddy of time *t*. The eddy migration velocity is defined as the average velocity of the eddies those last one week or more in the study area; the migration velocity of summer cyclone is 5.64 cm/s and anticyclone is 5.71 cm/s. The rotation velocity of the mesoscale oceanic eddy is the average velocity of the detected eddy edges. The critical depth where the nonlinear constant reach 1 is defined as the trapped depth.

The climatological MLD ranges from 18.3 to 125.9 m. Figure 15 shows the distribution of trapped depth ranges from 20 to 130 m, the mean value of the trapped depth limiting from 20 to 130 m is deeper in cyclones than in anticyclones and so does the mean value of the trapped depth limiting from 100 to 130 m. Moreover, the anticyclones that only last one day outnumber the cyclones (7,913 to 6,425). The existence of a large number of weak anticyclones may be responsible for that less SLPVW and larger potential vorticity in the composite anticyclone.

6. Summary and Discussion

The correlation coefficient between the SSH and the volume of SLPVW in winter is positive in the north of 30°N and negative in the south of 30°N. However, in summer, this correlation is basically negative.

It is found that the eddy vorticity strength is the main cause of the north-south opposite distribution of the correlation coefficient in winter. The number of stronger anticyclones in the negative correlation value region is larger than those in the positive correlation value region. The abnormal THF of strong eddy is much stronger than usual. Therefore, it has a great influence on MLD. The large abnormal THF (more heat loss than usual) of the anticyclone can induce deep convection which is beneficial to generate thicker ML (namely, deeper MLD). Although the deeper MLD correspond to more low PV water generation, the low PV water that actually exists the subsurface ocean below the MLD (namely, SLPVW) is decreased due to the deeper MLD. The positive temperature anomaly decreases with the deepening of depth and the negative THF anomaly in the weak anticyclones, result in shallower MLD, and caused by the vertical decrease of warm advection; MLD shallows most in the northwestside of the composite weak anticyclone. Meanwhile, the horizontal gradient of MLD anomaly is much smaller than that in the strong anticyclone, resulting in a consistent increase of SLPVW in the weak anticyclone. On the contrary, the negative temperature anomaly of cyclone decreases with the deepening of depth, which is conducive to weaken the ocean stratification, and leads to deeper MLD in the weak cyclone where the THF anomaly is not very large, finally resulting in SLPVW decreasing in the weak cyclone.

To make the conclusions concerning oceanic eddies in winter more convincing, we add analyses of HYCOM/NCODA data from year 2001 to 2010 to compare with the NCEP-CFSR data. Similarly, we define the eddy with the vorticity in top 20 (bottom 20) percent in the study region in winter is strong-vorticity (weak vorticity) eddy in the HYCOM/NCODA. There are 17,085 anticyclones and 18,909 cyclones in the previous key region in winter without vorticity limit detected by the HYCOM/NCODA data from 2001 to 2010 (Figure 16). Similar with the eddy distribution of NCEP-CFSR data in winter, the stronger eddies are defined with the vorticity of anticyclone (cyclone) center is less (greater) than $-1.441{\cdot}10^{-5}$ s^{-1} ($1.431{\cdot}10^{-5}$ s^{-1}) (3,417 anticyclones and 3,781 cyclones). While the weaker eddies are defined with the vorticity of anticyclone (cyclone) center is greater (less) than $-5.466{\cdot}10^{-6}$ s^{-1} ($5.319{\cdot}10^{-6}$ s^{-1}) (3,417 anticyclones and 3,782 cyclones). The compositions between stronger and weaker winter eddies in the HYCOM/NCODA data (Figure 17) are just consistent with those of the NCEP-CFSR (Figure 6). Weaker anticyclone results in shallower MLD and thicker SLPVW, and the weaker cyclone results in deeper MLD and thinner SLPVW.

In winter, mesoscale oceanic eddies also have obvious impacts on the subduction rate. The time-averaged total subduction rate of the North Pacific from the year 1979 to 2010 is 5.15 Sv. While, the time-averaged eddy subduction rate is 1.88 Sv, which accounts for 36.4% of the total subduction rate. Furthermore, the variation of the total subduction rate is highly correlated with the numbers of anticyclone in the North Pacific.

In summer, mesoscale oceanic eddies mainly impact on the dissipation and retention of SLPVW. The NCEP-CFSR composition results in summer show that the volume of SLPVW increases in the composite cyclone but decreases in the composite anticyclone. And it is reconfirmed by the HYCOM/NCODA data in summer during years 2001–2010 (Figure 18). The three-dimensional structure of the composite eddy shows that the positive (negative) anomaly of divergence in the anticyclone (cyclone) decreases with depth growing, which results in the compression (stretching) of the distance between the adjacent isopycnic surfaces, leads to the

increasing (decreasing) of potential vorticity of the water masses between the adjacent isopycnic surfaces, finally accelerating (slowing down) the dissipation of SLPVW.

In addition, the statistical result of the trapped depth of summer eddies shows that the mean trapped depth of the anticyclone is larger than that of the cyclone, but there are a large number of weak anticyclones in the study region in summer, which may be responsible for that less SLPVW and higher potential vorticity in the composite anticyclone. How to distinguish the effects of different summer eddies with different vorticities needs to be addressed in the future research.

Acknowledgments
The authors thank the anonymous reviewers for their valuable comments and suggestions. This work has benefited from discussions with William Perrie of BIO. This work was supported by the National Key Program for Developing Basic Science (grants 2018YFC1505902 and 2016YFA0600303) and the National Natural Science Foundation of China (grants 41330420, 41621005, 41675064, 41675067, and 41875086). The authors are grateful to the support of the Jiangsu Provincial Innovation Center for Climate Change and Fundamental Research Funds for the Central University. This work was jointly supported by the Joint Open Project of KLME and CIC-FEMD (grant KLME201902). And the authors would like to thank Zhao Yihang and Deng Yuheng for data preparation. The NCEP Climate Forecast System Reanalysis 6-hourly data used in this study was obtained from the website (https://rda.ucar.edu/datasets/ds093.0/index.html#cgi-bin/datasets/getWebList?dsnum = 093.0&ls = 0&sessID = Je4dk1fOcgEmlONwmHQeJvebgxqcY-H&action = doGrMLQuery&sort = &ptfile = &ll = 500&iv = &scrollTop = 23506&preset = &disp=). The Global HYbrid Coordinate Ocean Model and the Navy Coupled Ocean Reanalysis Data used in this study was obtained from the website (http://tds.HYCOM/NCODA.org/thredds/catalogs/GLBv0.08/expt_53.X.html).

References

Bai, H., Hu, H., Yang, X., Ren, X., Xu, H., & Liu, G.-Q. (2019). Modeled MABL responses to the winter Kuroshio SST front in the East ChinaSea and Yellow Sea. *Journal of Geophysical Research: Atmospheres*, *124*. https://doi.org/10.1029/2018JD029570

Bates, N. R., Pequignet, A. C., Johnson, R. J., & Gruber, N. (2003). A variable sink for atmospheric CO_2 in subtropical mode water of the North Atlantic Ocean. Nature[J]. *Nature*, *420*(6915), 489–493.

Chang, R., & Zhang, Q. Y. (2010). Relationship between the North Pacific subtropical mode water anomaly in summer and the interannual change of autumn-winter air temperature over China[J]. *climatological & Environmental Research*, *15*(3), 303–310.

Chen, Q., Hu, H., Ren, X., & Yang, X.-Q. (2019). Numerical simulation of midlatitude upper-level zonal wind response to the change of North Pacifificsubtropical front strength. *Journal of Geophysical Research: Atmospheres*, *124*. https://doi.org/10.1029/2018JD029589

Chelton, D. B., Schlax, M. G., Samelson, R. M., & deSzoeke, R. A. (2007). Global observations of large oceanic eddies[J]. *Geophysical Research Letters*, *34*, L15606. https://doi.org/10.1029/2007GL030812

Endoh, T., Jia, Y., & Richards, K. J. (2006). Sensitivity of the ventilation process in the North Pacific to eddy-induced tracer transport. *Journal of Physical Oceanography*, *36*, 1895–1911.

Flierl, G. R. (1981). Particle motions in large-amplitude wave fields[J]. *Geophysical and Astrophysical Fluid Dynamics*, *18*(1-2), 39–74.

Hautala, S., & Roemmich, D. (1998). Subtropical mode water in the Northeast Pacific basin [J]. *Geophys Res*, *103*, 13,055–13,066.

Kobashi, F., & Kubokawa, A. (2012). Review on North Pacific subtropical countercurrents and subtropical fronts: Role of mode waters in ocean circulation and climate[J]. *Journal of Oceanography*, *68*(1), 21–43.

Kouketsu, S., Tomita, H., Oka, E., Hosoda, S., Kobayashi, T., & Sato, K. (2011). The role of meso-scale eddies in mixed layer deepening and mode water formation in the western North Pacific[M]//New Developments in Mode-Water Research. *Springer Japan*, 59–73.

Kremeur, A., Levy, M., Aumont, O., & Reverdin, G. (2009). Impact of the subtropical mode water biogeochemical properties on primary production in the North Atlantic: New insights from an idealized model study[J]. *Journal of Geophysical Research*, *114*, C07019. https://doi.org/10.1029/2008JC005161

Liu, C., & Peiliang, L. I. (2013). The impact of meso-scale eddies on the subtropical mode water in the western North Pacific[J]. *Journal of Ocean University of China*, *12*(2), 230–236.

Liu, Q., & Hu, H. (2007). A subsurface pathway for low potential vorticity transport from the central North Pacific toward Taiwan Island[J]. *Geophysical Research Letters*, *34*, L12710. https://doi.org/10.1029/2007GL029510

Marshall, J. C., Nurser, A. J. G., & Williams, R. G. (1993). Inferring the subduction rate and period over the North Atlantic. *Journal of Physical Oceanography*, *23*, 1315–1329.

Masuzawa, J. (1969). Subtropical mode water [J]. *Deep Sea Research and Oceanographic Abstracts*, *16*(5), 463–468.

Nakamura, H. (1996). A pycnostad on the bottom of the ventilated portion in the central subtropical North Pacific: Its distribution and formation [J]. *Oceanography*, *52*, 171–188.

Nencioli, F., Dong, C., Dickey, T., Washburn, L., & McWilliams, J. C. (2010). A vector geometry based eddy detection algorithm and its application to high-resolution numerical model products and High-Frequency radar surface velocities in the Southern California Bight [J]. *Atmos. Ocean. Tech.*, *27*(3), 564–579. https://doi.org/10.1175/2009JTECHO725.1

Nishikawa, S., Tsujino, H., Sakamoto, K., & Nakano, H. (2010). Effects of mesoscale oceanic eddies on subduction and distribution of subtropical mode water in an eddy-resolving OGCM of the western North Pacific[J]. *Journal of Physical Oceanography*, *40*(8), 1748–1765. https://doi.org/10.1175/2010JPO4261.1

Oka, E., & Qiu, B. (2012). Progress of North Pacific mode water research in the past decade[J]. *Journal of Oceanography*, *68*(1), 5–20.

Oka, E., Suga, T., Sukigara, C., Toyama, K., Shimada, K., & Yoshida, J. (2011). "Eddy resolving" observation of the North Pacific subtropical mode water[J]. *Journal of Physical Oceanography*, *41*(4), 666–681.

Pan, A., & Liu, Q. (2005). Mesoscale oceanic eddy effects on the wintertime vertical mixing in the formation region of the North Pacific Subtropical Mode Water[J]. *Science Bulletin*, *50*(17), 1949–1956.

Qiu, B. (2002). The Kuroshio extension system: Its large-scale variability and role in the midlatitude ocean-atmosphere interaction[J]. *Journal of Oceanography*, *58*(1), 57–75.

Qiu B.[2], Chen S., Hacker P. (2006). Effect of mesoscale oceanic eddies on subtropical mode water variability from the Kuroshio extension system study (KESS)[J]. *Journal of Physical Oceanography* *37*(4):982.

Qiu B.[1] , Hacker P., Chen S, Donohue K. A., Watts D. R., Mitsudera H., et al. (2006). Observations of the subtropical mode water evolution from the Kuroshio extension system study[J]. *Journal of Physical Oceanography*, *36*(3):457-473. https://doi.org/10.1175/JPO2849.1.

Qiu, B., & Huang, R. X. (1995). Ventilation of the North Atlantic and North Pacific: Subduction versus obduction[J]. *Journal of Physical Oceanography*, *25*(10), 2374–2390.

Rainville, L., Jayne, S. R., Mcclean, J. L., & Maltrud, M. E. (2007). Formation of subtropical mode water in a high-resolution ocean simulation of the Kuroshio extension region[J]. *Ocean Modelling*, *17*(4), 338–356. https://doi.org/10.1016/j.ocemod.2007.03.002

Saha, S., Moorthi, S., Pan, H. L., Wu, X., Wang, J., Nadiga, S., et al. (2010). The NCEP climate forecast system reanalysis[J]. *Bulletin of the American Meteorological Society*, *91*(8), 1015–1058. https://doi.org/10.1175/2010BAMS3001.1

Shi, F., Luo, Y., & Xu, L. (2018). Volume and transport of eddy-trapped mode water south of the Kuroshio extension. *Journal of Geophysical Research: Oceans*, *123*(12), 8749–8761.

Song, X. Z., Lin, X. P., Padmore, M. R., Zheng, P. N., & Qian, H. (2009). Spacial structure and annual variation estimated from Argo float data for subtropical mode water in the northwest Pacific Ocean[J]. *Advances in Marine Science*.

Stommel, H. (1979). Determination of water mass properties of water pumped down from the Ekman layer to the geostrophic flow below [J]. *Proceedings of the National Academy of Sciences of the United States of America*, *76*(7), 3051–3055. https://doi.org/10.1073/pnas.76.7.3051

Suga, T., Takei, Y., & Hanawa, K. (1997). Thermostad distribution in the North Pacific subtropical gyre: The central mode water and the subtropical mode water[J]. *Physical Oceanography*, *27*, 140–152.

Sukigara, C., Suga, T., Saino, T., Toyama, K., Yanagimoto, D., Hanawa, K., & Shikama, N. (2011). Biogeochemical evidence of large diapycnal diffusivity associated with the subtropical mode water of the North Pacific. *Journal of Oceanography*, *67*, 77–85.

Uehara, H., Suga, T., Hanawa, K., & Shikama, N. (2003). A role of eddies in formation and transport of North Pacific Subtropical Mode Water[J]. *Geophysical Research Letters*, *30*(13), 1705. https://doi.org/10.1029/2003GL017542

Xie, S. P., Xu, L., Liu, Q., & Kobashi, F. (2011). Dynamical role of mode water ventilation in decadal variability in the central subtropical gyre of the North Pacific[J]. *Journal of Climate*, *24*(4), 1212–1225. https://doi.org/10.1175/2010JCLI3896.1

Xu, L., Li, P., Xie, S. P., Liu, Q., Liu, C., & Gao, W. (2016). Observing mesoscale eddy effects on mode-water subduction and transport in the North Pacific[J]. *Nature Communications*, *7*(1), 10505. https://doi.org/10.1038/ncomms10505

Xu, L., Xie, S. P., & Liu, Q. (2012). Mode water ventilation and subtropical countercurrent over the North Pacific in CMIP5 simulations and future projections[J]. *Journal of Geophysical Research, Oceans*, *117*(C12).

Xu, L., Xie, S. P., Liu, Q., Liu, C., Li, P., & Lin, X. (2017). Evolution of the North Pacific subtropical mode water in anticyclonic eddies[J]. *Journal of Geophysical Research: Oceans*, *122*, 10,118–10,130. https://doi.org/10.1002/2017JC013450

Xu, L., Xie, S. P., Mcclean, J. L., Liu, Q., & Sasaki, H. (2014). Mesoscale eddy effects on the subduction of North Pacific mode waters[J]. *Journal of Geophysical Research: Oceans*, *119*, 4867–4886. https://doi.org/10.1002/2014JC009861